Journal of Electronics and Electrical Engineering
https://ojs.wiserpub.com/index.php/JEEE/

Research Article

Modeling and Simulation of a Single-Phase Linear Multi-Winding Transformer in the d-q Frame

José M. Campos-Salazar[1*], Ariel Viani-Abad[2], Rodrigo Sandoval-García[3]

[1]Department of Electronic Engineering, Universitat Politècnica de Catalunya, Barcelona, Spain
[2]Department of Control Engineering, Tecnómade, Concepción, Chile
[3]Department of Control Engineering, Arauco y Constitución Mill, Concepción, Chile
E-mail: jose.campos.salazar@upc.edu

Received: 29 February 2024; **Revised:** 6 May 2024; **Accepted:** 13 May 2024

Abstract: Exploring the fundamental principles of system modeling in electrical engineering, this study delves into the transformative power of the d-q transformation, highlighting its pivotal role in rendering time-varying systems into a coherent steady-state representation. Departing from conventional approaches, the study navigates the complexities of single-phase transformer configurations, utilizing the Clarke and Park transformations to seamlessly transition between electrical coordinates and the d-q frame. Through extensive derivations, dynamic equations are formulated in both α-β and d-q coordinates, providing a detailed understanding of system dynamics under specific loads. In addition, the study extends the analysis to a generalized multi-winding transformer model that accommodates a wide range of transformer setups. With detailed mathematical derivations, insightful visual aids, and clear state-space representations, this work attempt to be a resource for researchers seeking to unravel the intricacies of electrical system modeling and analysis.

Keywords: d-q transformation, system modeling, electrical engineering, clarke transformation, park transformation, state-space representation, single-phase transformers, dynamic equations, steady-state analysis, generalized model

1. Introduction

The increase in the adoption of electric vehicles (EVs) reflects the growing global concern for environmental sustainability and energy efficiency. This shift requires a deep understanding of crucial components in electric power systems, specifically transformers (TRs), which have a crucial role in power distribution and conversion processes. Numerous studies have explored the modeling and simulation of TRs, including both single-phase and three-phase configurations. However, the existing literature presents a variety of modeling techniques, ranging from classical phasor-based representations to more contemporary state-space formulations [1, 2, 3, 4, 5, 6, 7, 8, 9, 10, 11, 12].

The increasing need for standard (two-level) and multilevel power dc-dc converters with galvanic isolation highlights the importance of precise TR models in various applications, such as renewable energy systems, telecommunications infrastructure, data centers, electric vehicle charging networks, battery energy storage systems, microgrids, and power distribution networks [13]. The integration of TRs within dc-dc converters, such as dual-active-bridge converters (DABs) and solid-state transformers (SSTs), highlights their versatile utility and prominence in modern power electronics [7, 12].

DOI: https://doi.org/10.37256/jeee.3120244530

Traditional approaches to TR modeling often focus on sinusoidal steady-state analysis using phasor techniques in the frequency domain. However, as system complexity in-creases, especially with configurations involving multiple secondary windings while retaining a single primary winding, the dynamic modeling of TRs becomes inherently intricate. In such scenarios, alternative analysis methodologies are necessary, particularly for linear circuits. State-space analysis is a promising approach for characterizing multiple-input multiple-output systems. State-space models provide a concise and efficient representation, which facilitates streamlined analysis and reduces computational overhead during simulation [14, 15].

In applications that use DABs or SSTs, it is undeniable that control systems must regulate voltage or current output [7, 12, 16, 17, 18]. However, synthesizing control systems for such applications is inherently challenging due to the nonlinear nature of these systems. They are characterized by switching functions and time-varying variables, despite operating in a steady state. To address this challenge, it is necessary to linearize these systems and derive small-signal models that are conducive to the synthesis of linear compensators [19, 20]. One prevalent approach is to use the d-q transformation to effectively treat the time-varying variables associated with TRs, making them like a dc system with constant values during the stationary regime [21].

However, the search for a linear small-signal model in d-q coordinates, which would allow for the use of linear feedback output compensators for system control, requires a comprehensive model for TRs with multiple secondary windings. Unfortunately, such a model is currently absent from the literature. The objective of this paper is to develop a generalized model for a single-phase transformer with z-secondary windings that exhibit constant behavior over time. The model utilizes transformation in the d-q frame and is suitable for implementing linear feedback output regulators, such as a PI regulator or a linear-quadratic regulator. While this paper does not detail or synthesize a linear regulator, it provides a detailed explanation of the process for obtaining the model.

Nevertheless, most of the articles in the literature that refer to transformer models in the d-q frame refer to three-phase electrical transformers [21, 22, 23, 24]; very few studies cover the modeling of single-phase transformers in the d-q frame with a single primary and secondary winding [25, 26], but there is no reference to this type of modeling for generalized systems (z secondary windings).

To derive this generalized model, a TR with a single primary winding and a single secondary winding is first modeled in electrical coordinates and then transformed into d-q coordinates. Next, this methodology is extended to TR configurations with one primary winding and multiple secondary windings, culminating in a comprehensive model that includes both electrical and d-q coordinates.

To validate the proposed model, different TR configurations are implemented using two simulation environments: the power electronics simulator PSIM and the MATLAB-Simulink platform. These configurations included primary windings with one, two, and three secondary windings, allowing for a robust evaluation of the model's accuracy. Comparative analysis between the simulated electrical variables and the derived model is performed to assess the fidelity and effectiveness of the model.

This research aims to address the gap in the literature regarding a generalized d-q coordinate small-signal state-space linear model for TRs with multiple secondary windings. The proposed model's accuracy and utility are analyzed through simulation and validation efforts, thus leading the way to a better understanding and optimization of TR-based systems in various applications.

The following sections discuss the topologies of the examined TRs, explain the process of TR modeling in both electrical and d-q coordinates, and present the methodology used to derive the generalized small-signal state-space linear model. This is followed by a comprehensive validation analysis.

The article is structured as follows: sections two, three, and four illustrate the topologies of the TRs under study, detail the modeling of the TRs in electrical and d-q coordinates, and analyze the simulation results, respectively. Sections five, six, and seven present the simulation results, give the solution of the dynamical equations of the models under study, and the conclusion are given, respectively.

2. Transformer topology

The functionality and performance of TRs are significantly influenced by their topology. This chapter explains the TR topologies proposed in this study, highlighting the essential characteristics and configurations required for subsequent modeling and analysis.

2.1 *Overview of transformer topologies*

Figure 1 shows the TR topologies proposed for consideration in this article. These TRs have a primary winding (winding 11) and multiple secondary windings (windings 21, 22, and 2z, where $z \in \mathbb{N}$). It is important to note that, following standard modeling conventions [14, 27], the mutual inductances between the primary winding and each of the secondary windings, as well as between the secondary windings themselves, are not considered. The analysis that follows excludes coupled circuit models [28]. Also, in this study, it is assumed that there is a linear relationship between the flux variables and the magnetomotive force, and therefore the transformers used in this study are manufactured from linear ferromagnetic iron [14, 29, 30].

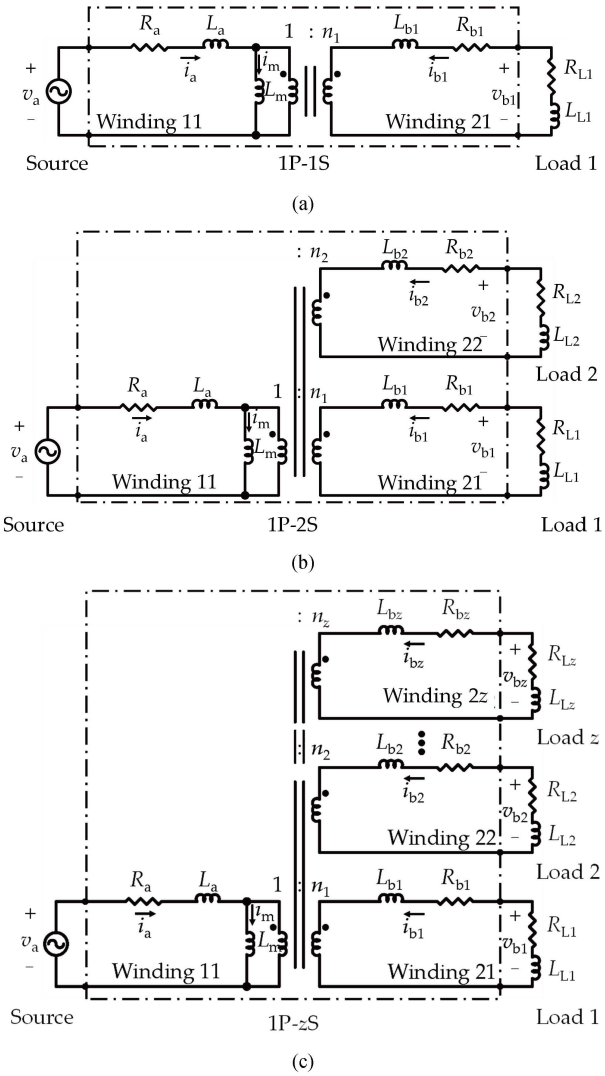

Figure 1. Equivalent circuit of different TRs. (**a**) 1P-1S. (**b**) 1P-2S. (**c**) 1P-zS.

2.2 *Specific transformer configurations*

- 1P-1S configuration (Figure 1a): This configuration features a primary winding (winding 11) and a single secondary winding (winding 21).
- 1P-2S configuration (Figure 1b): The 1P-2S TR configuration incorporates a primary winding and two secondary windings (windings 21 and 22).
- Generalized TR (1P-zS) configuration (Figure 1c): This configuration entails a primary winding (winding 11) and z secondary windings (windings 21, 22, …, and 2z).

2.3 *Electrical characteristics*

All proposed TR models shown in Figure 1 feature the primary common winding (winding 11), which is characterized by its (L_{a}). The model also accounts for the core excitation effect through the magnetizing inductance (L_{m}), while omitting magnetizing losses.

The model considers the ohmic losses ($R_{\mathrm{b}x}$) and leakage inductances ($L_{\mathrm{b}x}$) of each individual secondary winding ($x \in \{1, 2, ..., z\}$). Additionally, the loads are modeled as an R-L branch with $R_{\mathrm{L}x}$ and $L_{\mathrm{L}x}$. The electrical variables for winding 11 consist of the input terminal voltage (v_{a}), input terminal current (i_{a}), and magnetizing current (i_{m}). The electrical variables of windings 21 (1P-1S), 22 (1P-2S), and 2z (1P-zS) are the output terminal voltage ($v_{\mathrm{b}z}$) and output terminal current ($i_{\mathrm{b}z}$), respectively. The transformer turns ratio, defined as $1/n_z$ where n_z corresponds to the number of turns in the secondary winding z, is represented by $t_{\mathrm{r}z}$.

3. System modeling in electrical coordinates

This section aims to develop the dynamic model of the proposed TR topology shown in Figure 1c, specifically the 1P-zS configuration, in electrical coordinates (ec). The dynamic model is expressed in the observable canonical form as a state-space representation [19], which facilitates subsequent analysis and simulation.

3.1 *Dynamic model derivation: 1P-1S configuration*

The derivation begins with the 1P-1S model, using the same methodology used for representing the 1P-1S configuration. The dynamic equations for the 1P-1S configuration, shown in Figure 1a, are defined in vector-matrix form as follows [14]:

$$\mathbf{L} \cdot \mathrm{d}\mathbf{x}/\mathrm{d}t = \mathbf{V} \tag{1}$$

$$\mathbf{L} = \begin{bmatrix} L_{\mathrm{a}} & 0 & L_{\mathrm{m}} \\ 0 & L_{\mathrm{b}_1} & \frac{L_{\mathrm{m}}}{t_{\mathrm{r}_1}} \\ 1 & \frac{1}{t_{\mathrm{r}_1}} & -1 \end{bmatrix}, \quad \mathbf{x} = \begin{bmatrix} i_{\mathrm{a}} \\ i_{\mathrm{b}_1} \\ i_{\mathrm{m}} \end{bmatrix}, \quad \mathbf{V} = \begin{bmatrix} v_{\mathrm{a}} - R_{\mathrm{a}} \cdot i_{\mathrm{a}} \\ v_{\mathrm{b}_1} - R_{\mathrm{b}_1} \cdot i_{\mathrm{b}_1} \\ 0 \end{bmatrix} \tag{2}$$

where $t_{\mathrm{r}1} = 1/n_1$. The dynamic equations for the 1P-1S system are defined by solving for $\mathrm{d}\mathbf{x}/\mathrm{d}t$ and setting the solutions as functions:

$$\begin{cases} \frac{\mathrm{d}i_{\mathrm{a}}}{\mathrm{d}t} = f_1(\mathbf{u}, \mathbf{x}) \\ \frac{\mathrm{d}i_{\mathrm{b}_1}}{\mathrm{d}t} = f_2(\mathbf{u}, \mathbf{x}) \\ \frac{\mathrm{d}i_{\mathrm{m}}}{\mathrm{d}t} = f_3(\mathbf{u}, \mathbf{x}) \end{cases} \tag{3}$$

In this context, $\mathbf{u} = [u_1, u_2]^{\mathrm{T}} = [v_{\mathrm{a}}, v_{\mathrm{b}1}]^{\mathrm{T}}$, and $\mathbf{x} = [x_1, x_2, x_3]^{\mathrm{T}} = [i_{\mathrm{a}}, i_{\mathrm{b}1}, i_{\mathrm{m}}]^{\mathrm{T}}$ represent the input and state vectors respectively, where $\mathbf{u} \in \{\mathbb{R}^2\}$ and $\mathbf{x} \in \{\mathbb{R}^3\}$. By grouping the functions $f_1(\mathbf{u}, \mathbf{x})$, $f_2(\mathbf{u}, \mathbf{x})$, and $f_3(\mathbf{u}, \mathbf{x})$ into the vector $\mathbf{f} = [f_1(\mathbf{u}, \mathbf{x}), f_2(\mathbf{u}, \mathbf{x}), f_3(\mathbf{u}, \mathbf{x})]^{\mathrm{T}}$, where $\mathbf{f} \in \{\mathbb{R}^3\}$ and defining the output vector as $\mathbf{y} = \mathbf{x}$, the state-space model of the 1P-1S in ec is obtained and shown as follows:

$$\begin{cases} \dot{\mathbf{x}} = \mathbf{A_{ec}} \cdot \mathbf{x} + \mathbf{B_{ec}} \cdot \mathbf{u} \\ \mathbf{y} = \mathbf{C_{ec}} \cdot \mathbf{x} + \mathbf{D_{ec}} \cdot \mathbf{u} \end{cases} \tag{4}$$

The state matrix $\mathbf{A_{ec}}$, the input matrix $\mathbf{B_{ec}}$, the output matrix $\mathbf{C_{ec}}$, and the direct-transmission matrix $\mathbf{D_{ec}}$, and are defined as follows:

$$\begin{aligned} \mathbf{A_{ec}} &= \begin{bmatrix} \frac{\partial f_1(\mathbf{u},\mathbf{x})}{\partial x_1} & \frac{\partial f_1(\mathbf{u},\mathbf{x})}{\partial x_2} & \frac{\partial f_1(\mathbf{u},\mathbf{x})}{\partial x_3} \\ \frac{\partial f_2(\mathbf{u},\mathbf{x})}{\partial x_1} & \frac{\partial f_2(\mathbf{u},\mathbf{x})}{\partial x_2} & \frac{\partial f_2(\mathbf{u},\mathbf{x})}{\partial x_3} \\ \frac{\partial f_3(\mathbf{u},\mathbf{x})}{\partial x_1} & \frac{\partial f_3(\mathbf{u},\mathbf{x})}{\partial x_2} & \frac{\partial f_3(\mathbf{u},\mathbf{x})}{\partial x_3} \end{bmatrix} = \left[\frac{\partial f_i(\mathbf{u},\mathbf{x})}{\partial x_j}\right], \\ \mathbf{B_{ec}} &= \begin{bmatrix} \frac{\partial f_1(\mathbf{u},\mathbf{x})}{\partial u_1} & \frac{\partial f_1(\mathbf{u},\mathbf{x})}{\partial u_2} \\ \frac{\partial f_2(\mathbf{u},\mathbf{x})}{\partial u_1} & \frac{\partial f_2(\mathbf{u},\mathbf{x})}{\partial u_2} \\ \frac{\partial f_3(\mathbf{u},\mathbf{x})}{\partial u_1} & \frac{\partial f_3(\mathbf{u},\mathbf{x})}{\partial u_2} \end{bmatrix} = \left[\frac{\partial f_i(\mathbf{u},\mathbf{x})}{\partial u_k}\right], \\ \mathbf{C_{ec}} &= \begin{bmatrix} \frac{\partial x_1}{\partial x_1} & \frac{\partial x_1}{\partial x_2} & \frac{\partial x_1}{\partial x_3} \\ \frac{\partial x_2}{\partial x_1} & \frac{\partial x_2}{\partial x_2} & \frac{\partial x_2}{\partial x_3} \\ \frac{\partial x_3}{\partial x_1} & \frac{\partial x_3}{\partial x_2} & \frac{\partial x_3}{\partial x_3} \end{bmatrix} = \left[\frac{\partial x_i}{\partial x_j}\right], \ \mathbf{D_{ec}} = \begin{bmatrix} \frac{\partial x_1}{\partial u_1} & \frac{\partial x_1}{\partial u_2} \\ \frac{\partial x_2}{\partial u_1} & \frac{\partial x_2}{\partial u_2} \\ \frac{\partial x_3}{\partial u_1} & \frac{\partial x_3}{\partial u_2} \end{bmatrix} = \left[\frac{\partial x_i}{\partial u_k}\right] \\ &\forall \{i,j\} \in \{1,2,3\} \ \text{ and } \ k \in \{1,2\} \end{aligned} \tag{5}$$

Furthermore, $\{\mathbf{A_{ec}}, \mathbf{C_{ec}}\} \in \mathscr{M}_{3\times 3}$ {K} and $\{\mathbf{B_{ec}}, \mathbf{D_{ec}}\} \in \mathscr{M}_{3\times 2}$ {K}. It is important to note that the partial differential operators presented in (5) are not related to the linearization procedure involving partial derivatives around operating points calculated during steady-state operation [19]. The description in (5) merely shows a simple calculation to obtain such matrices The load 1 model regarding to Figure 1a is defined by:

$$v_{\mathrm{b}_1} = -\left(R_{\mathrm{L}_1} \cdot i_{\mathrm{b}_1} + L_{\mathrm{L}_1} \cdot \frac{\mathrm{d}i_{\mathrm{b}_1}}{\mathrm{d}t}\right) \tag{6}$$

Figure 2a illustrates the state-space diagram in ec, in combination with the load 1 model. Equations (4) and (6) represent the state-space and load models, respectively, in the controllable canonical form for the 1P-1S system.

3.2 *Dynamic model derivation: 1P-2S configuration*

The methodology is extended to derive the vector-matrix dynamic model for the 1P-2S system in ec. The dynamic equations related to this configuration are derived similarly to the 1P-1S system, considering Figure 1b. The dynamic model is expressed as follows:

$$\mathbf{L} = \begin{bmatrix} L_{\mathrm{a}} & 0 & 0 & L_{\mathrm{m}} \\ 0 & L_{\mathrm{b}_1} & 0 & \frac{L_{\mathrm{m}}}{t_{\mathrm{r}_1}} \\ 0 & 0 & L_{\mathrm{b}_2} & \frac{L_{\mathrm{m}}}{t_{\mathrm{r}_2}} \\ 1 & \frac{1}{t_{\mathrm{r}_1}} & \frac{1}{t_{\mathrm{r}_2}} & -1 \end{bmatrix}, \quad \mathbf{x} = \begin{bmatrix} i_{\mathrm{a}} \\ i_{\mathrm{b}_1} \\ i_{\mathrm{b}_2} \\ i_{\mathrm{m}} \end{bmatrix}, \quad \mathbf{V} = \begin{bmatrix} v_{\mathrm{a}} - R_{\mathrm{a}} \cdot i_{\mathrm{a}} \\ v_{\mathrm{b}_1} - R_{\mathrm{b}_1} \cdot i_{\mathrm{b}_1} \\ v_{\mathrm{b}_2} - R_{\mathrm{b}_2} \cdot i_{\mathrm{b}_2} \\ 0 \end{bmatrix} \tag{7}$$

The set of dynamic equations for the 1P-2S system is given by:

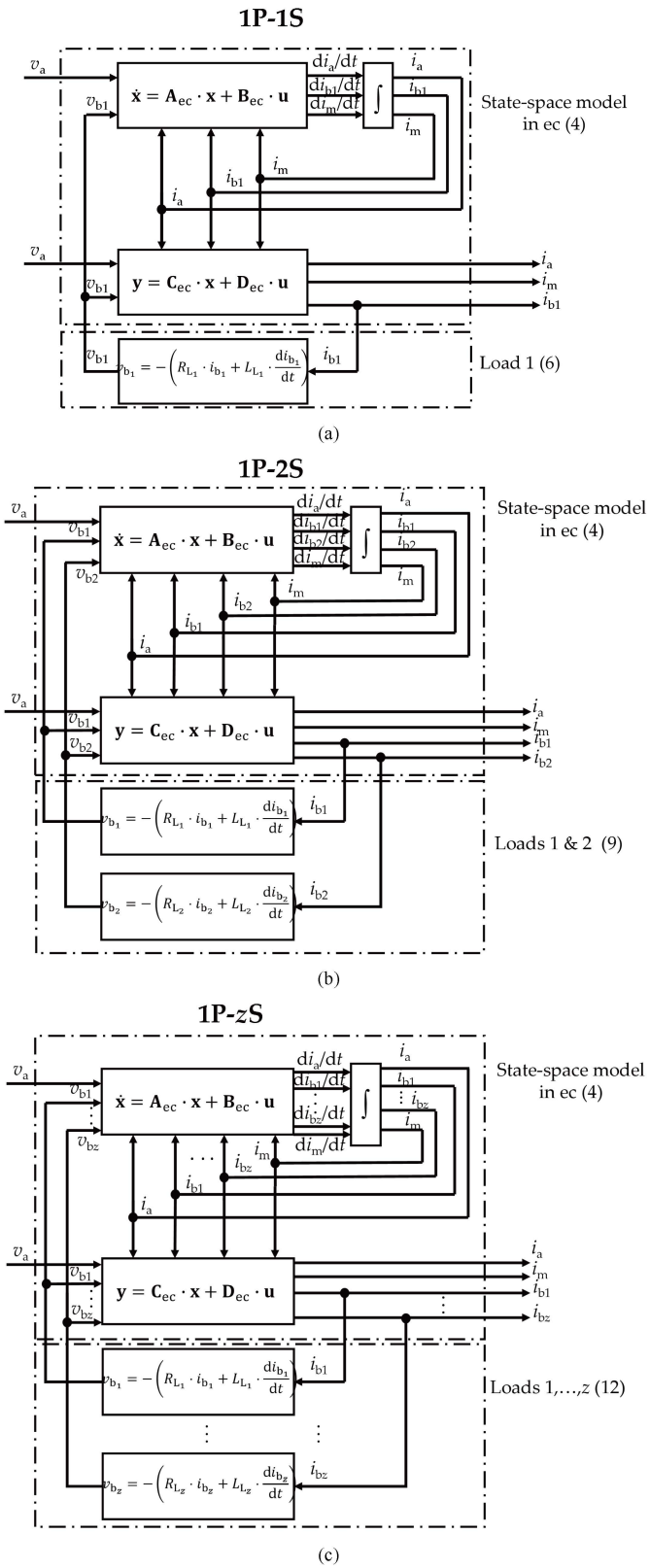

Figure 2. State-space models in ec of different TRs. (**a**) 1P-1S. (**b**) 1P-2S. (**c**) 1P-zS.

$$\begin{cases} \frac{\mathrm{d}i_{\mathrm{a}}}{\mathrm{d}t} = f_1(\mathbf{u},\mathbf{x}) \\ \frac{\mathrm{d}i_{\mathrm{b}_1}}{\mathrm{d}t} = f_2(\mathbf{u},\mathbf{x}) \\ \frac{\mathrm{d}i_{\mathrm{b}_2}}{\mathrm{d}t} = f_3(\mathbf{u},\mathbf{x}) \\ \frac{\mathrm{d}i_{\mathrm{m}}}{\mathrm{d}t} = f_4(\mathbf{u},\mathbf{x}) \end{cases} \tag{8}$$

The models of loads 1 and 2, according to Figure 1b, are specified as follows:

$$\begin{cases} v_{\mathrm{b}_1} = -\left(R_{\mathrm{L}_1}\cdot i_{\mathrm{b}_1} + L_{\mathrm{L}_1}\cdot\frac{\mathrm{d}i_{\mathrm{b}_1}}{\mathrm{d}t}\right) \\ v_{\mathrm{b}_2} = -\left(R_{\mathrm{L}_2}\cdot i_{\mathrm{b}_2} + L_{\mathrm{L}_2}\cdot\frac{\mathrm{d}i_{\mathrm{b}_2}}{\mathrm{d}t}\right) \end{cases} \tag{9}$$

From here, $\mathbf{u} = [u_1, u_2, u_3]^{\mathrm{T}} = [v_{\mathrm{a}}, v_{\mathrm{b}1}, v_{\mathrm{b}2}]^{\mathrm{T}}$, and $\mathbf{x} = [x_1, x_2, x_3, x_4]^{\mathrm{T}} = [i_{\mathrm{a}}, i_{\mathrm{b}1}, i_{\mathrm{b}2}, i_{\mathrm{m}}]^{\mathrm{T}}$. Additionally, $\mathbf{u} \in \{\mathbb{R}^3\}$ and $\mathbf{x} \in \{\mathbb{R}^4\}$. Taking (7) into account, $t_{\mathrm{r}2} = 1/n_2$. The function vector $\mathbf{f} = [f_1(\mathbf{u}, \mathbf{x}), f_2(\mathbf{u}, \mathbf{x}), f_3(\mathbf{u}, \mathbf{x}), f_4(\mathbf{u}, \mathbf{x})]^{\mathrm{T}}$, where $\mathbf{f} \in \{\mathbb{R}^4\}$, is defined. Considering $\mathbf{y} = \mathbf{x}$, the state-space model of the 1P-2S system in ec is derived in (4). The matrices $\mathbf{A_{ec}}$, $\mathbf{B_{ec}}$, $\mathbf{C_{ec}}$, and $\mathbf{D_{ec}}$ are defined in (5) where $\{i, j\} \in \{1, 2, 3, 4\}$ and $k \in \{1, 2, 3\}$. Also $\{\mathbf{A_{ec}}, \mathbf{C_{ec}}\} \in \mathscr{M}_{4\times 4}$ {K} and $\{\mathbf{B_{ec}}, \mathbf{D_{ec}}\} \in \mathscr{M}_{4\times 3}$ {K}. Figure 2b presents the state-space diagram in ec, combined with the models of loads 1 and 2. Equations (4) and (9) represent the state-space and load models, respectively, in the controllable canonical form for the 1P-2S system.

3.3 *Dynamic model derivation: generalized 1P-zS configuration*

The dynamic model for the generalized 1P-zS configuration, as shown in Figure 1c, is defined in a similar manner. The dynamic equations are expressed in vector-matrix form, considering the z secondary windings. The model is given by:

$$\mathbf{L} = \begin{bmatrix} L_{\mathrm{a}} & 0 & 0 & 0 & \cdots & 0 & L_{\mathrm{m}} \\ 0 & L_{\mathrm{b}_1} & 0 & 0 & \cdots & 0 & \frac{L_{\mathrm{m}}}{t_{\mathrm{r}_1}} \\ 0 & 0 & L_{\mathrm{b}_2} & 0 & \cdots & 0 & \frac{L_{\mathrm{m}}}{t_{\mathrm{r}_2}} \\ 0 & 0 & 0 & L_{\mathrm{b}_3} & \cdots & 0 & \frac{L_{\mathrm{m}}}{t_{\mathrm{r}_3}} \\ \vdots & \vdots & \vdots & \vdots & \ddots & \vdots & \vdots \\ 0 & 0 & 0 & 0 & \cdots & L_{\mathrm{b}_z} & \frac{L_{\mathrm{m}}}{t_{\mathrm{r}_z}} \\ 1 & \frac{1}{t_{\mathrm{r}_1}} & \frac{1}{t_{\mathrm{r}_2}} & \frac{1}{t_{\mathrm{r}_3}} & \cdots & \frac{1}{t_{\mathrm{r}_z}} & -1 \end{bmatrix}, \quad \mathbf{x} = \begin{bmatrix} i_{\mathrm{a}} \\ i_{\mathrm{b}_1} \\ i_{\mathrm{b}_2} \\ i_{\mathrm{b}_3} \\ \vdots \\ i_{\mathrm{b}_z} \\ i_{\mathrm{m}} \end{bmatrix}, \quad \mathbf{V} = \begin{bmatrix} v_{\mathrm{a}} - R_{\mathrm{a}}\cdot i_{\mathrm{a}} \\ v_{\mathrm{b}_1} - R_{\mathrm{b}_1}\cdot i_{\mathrm{b}_1} \\ v_{\mathrm{b}_2} - R_{\mathrm{b}_2}\cdot i_{\mathrm{b}_2} \\ v_{\mathrm{b}_3} - R_{\mathrm{b}_3}\cdot i_{\mathrm{b}_3} \\ \vdots \\ v_{\mathrm{b}_z} - R_{\mathrm{b}_z}\cdot i_{\mathrm{b}_z} \\ 0 \end{bmatrix} \tag{10}$$

The dynamic equations for the generalized 1P-zS system are given by (11). From here, $\mathbf{u} = [u_1, u_2, u_3, u_4, \ldots, u_z, u_{(z+1)}]^{\mathrm{T}} = [v_{\mathrm{a}}, v_{\mathrm{b}1}, v_{\mathrm{b}2}, v_{\mathrm{b}3}, ..., v_{\mathrm{b}z}]^{\mathrm{T}}$, and $\mathbf{x} = [x_1, x_2, x_3, x_4, \ldots, x_z, x_{(z+1)}, x_{(z+2)}]^{\mathrm{T}} = [i_{\mathrm{a}}, i_{\mathrm{b}1}, i_{\mathrm{b}2}, i_{\mathrm{b}3}, ..., i_{\mathrm{b}z}, i_{\mathrm{m}}]^{\mathrm{T}}$, with $\mathbf{u} \in \{\mathbb{R}^{(z+1)}\}$ and $\mathbf{x} \in \{\mathbb{R}^{(z+2)}\}$. From (10), $t_{rz} = 1/n_z$. By following the methodology employed in the previous analyzed cases, the vector function $\mathbf{f} = [f_1(\mathbf{u}, \mathbf{x}), f_2(\mathbf{u}, \mathbf{x}), f_3(\mathbf{u}, \mathbf{x}), ..., f_{z+1}(\mathbf{u}, \mathbf{x}), f_{z+2}(\mathbf{u}, \mathbf{x})]^{\mathrm{T}}$, where $\mathbf{f} \in \{\mathbb{R}^{(z+2)}\}$, is defined. Consequently, based on the vector $\mathbf{f}$, the state-space model in ec for the generalized system (1P-zS) is derived and expressed in (1). The matrices of the model are established in (5) where $i \in \{1, 2, \ldots, z\}$, $j \in \{1, 2, \ldots, z, \ldots, z{+}2\}$ and $k \in \{1, 2, \ldots, z{+}2\}$. Also $\{\mathbf{A_{ec}}, \mathbf{C_{ec}}\} \in \mathscr{M}_{(z+2)\times(z+2)}$ {K}, and $\{\mathbf{B_{ec}}, \mathbf{D_{ec}}\} \in \mathscr{M}_{(z+2)\times(z+1)}$ {K}.

$$\begin{cases} \frac{\mathrm{d}i_{\mathrm{a}}}{\mathrm{d}t} = f_1(\mathbf{u},\mathbf{x}) \\ \frac{\mathrm{d}i_{\mathrm{b}_1}}{\mathrm{d}t} = f_2(\mathbf{u},\mathbf{x}) \\ \frac{\mathrm{d}i_{\mathrm{b}_2}}{\mathrm{d}t} = f_3(\mathbf{u},\mathbf{x}) \\ \frac{\mathrm{d}i_{\mathrm{b}_3}}{\mathrm{d}t} = f_4(\mathbf{u},\mathbf{x}) \\ \vdots \\ \frac{\mathrm{d}i_{\mathrm{b}_z}}{\mathrm{d}t} = f_{z+1}(\mathbf{u},\mathbf{x}) \\ \frac{\mathrm{d}i_{\mathrm{m}}}{\mathrm{d}t} = f_{z+2}(\mathbf{u},\mathbf{x}) \end{cases} \tag{11}$$

The state-space model in ec for the generalized system (1P-zS) is derived similarly, resulting in (4) and the loads model are given by:

$$\begin{cases} v_{b_1} = -\left(R_{L_1} \cdot i_{b_1} + L_{L_1} \cdot \frac{di_{b_1}}{dt}\right) \\ v_{b_2} = -\left(R_{L_2} \cdot i_{b_2} + L_{L_2} \cdot \frac{di_{b_2}}{dt}\right) \\ v_{b_3} = -\left(R_{L_3} \cdot i_{b_3} + L_{L_3} \cdot \frac{di_{b_3}}{dt}\right) \\ \vdots \\ v_{b_z} = -\left(R_{L_z} \cdot i_{b_z} + L_{L_z} \cdot \frac{di_{b_z}}{dt}\right) \end{cases} \tag{12}$$

Finally, this section outlines the derivation of dynamic models for different configurations of a proposed TR topology. It begins with the 1P-1S configuration, proceeds to the 1P-2S configuration, and finally discusses the generalized 1P-zS configuration. Each derivation follows a clear methodology, expressing dynamic equations in vector-matrix form and defining state-space representations. The chapter presents equations and matrices in a systematic manner. However, additional explanations could enhance understanding, particularly for readers less familiar with the subject matter.

Overall, the section provides a solid foundation for analyzing the dynamic behavior of the proposed TR topology.

4. System modeling in d-q coordinates

In this section, the d-q model will be developed for each of the models, i.e., 1P-1S, and -2S, to obtain the generalized model 1P-zS in the d-q frame.

The d-q transformation is commonly used in electric/electronic systems [31, 32, 33, 34, 35, 36, 37] to convert time-varying systems, even in steady-state conditions, into a steady-state representation. However, the models proposed in Figure 1 are single-phase transformers, and therefore, the direct application of the d-q transformation is not feasible. Previous studies [26, 38, 39, 40] have addressed d-q coordinate conversions for single-phase electrical systems in system, selecting the electrical variables (v_a, v_{bx}, i_a, i_{bx}, and i_m where $x \in \{1, 2, \ldots, z\}$), and shifting them by 90 degrees. The phase-shifted variables are labeled as α and β (α-β coordinates) and rotate in the α-β plane. Once the system is in α-β coordinates, Park's transformation can be applied to obtain the final model in the d-q frame (static coordinates) [26].

Since the load is single-phase, the d-q coordinate system needs to be reconverted back into ec using the respective inverse transformations, i.e., from d-q to α-β, and then from α-β to ec.

Next, the d-q coordinate models for the 1P-1S system, the 1P-2S system, and the generalized 1P-zS model will be derived.

4.1 *Dynamic model derivation in d-q coordinates: 1P-1S configuration*

Following the procedure described above, the Clarke transformation is applied to the electrical variables in ec for the 1P-1S model, resulting in the variables transformed into α-β coordinates as given by:

$$\begin{bmatrix} v_{a_\alpha} \\ v_{a_\beta} \\ v_{b_{1\alpha}} \\ v_{b_{1\beta}} \end{bmatrix} = \begin{bmatrix} v_a(t) \\ v_a(t - \pi/2) \\ v_{b_1}(t) \\ v_{b_1}(t - \pi/2) \end{bmatrix}, \quad \begin{bmatrix} i_{a_\alpha} \\ i_{a_\beta} \\ i_{b_{1\alpha}} \\ i_{b_{1\beta}} \\ i_{m_\alpha} \\ i_{m_\beta} \end{bmatrix} = \begin{bmatrix} i_a(t) \\ i_a(t - \pi/2) \\ i_{b_1}(t) \\ i_{b_1}(t - \pi/2) \\ i_m(t) \\ i_m(t - \pi/2) \end{bmatrix} \tag{13}$$

By substituting (13) into (3), the set of dynamic equations in α-β coordinates are derived and given by

$$\begin{cases} \frac{\mathrm{d}i_{\mathrm{a}\alpha}}{\mathrm{d}t} = f_{\alpha\beta_1}\left(\mathbf{u}_{\boldsymbol{\alpha\beta}}, \mathbf{x}_{\boldsymbol{\alpha\beta}}\right) \\ \frac{\mathrm{d}i_{\mathrm{a}\beta}}{\mathrm{d}t} = f_{\alpha\beta_2}\left(\mathbf{u}_{\boldsymbol{\alpha\beta}}, \mathbf{x}_{\boldsymbol{\alpha\beta}}\right) \\ \frac{\mathrm{d}i_{\mathrm{b}1_\alpha}}{\mathrm{d}t} = f_{\alpha\beta_3}\left(\mathbf{u}_{\boldsymbol{\alpha\beta}}, \mathbf{x}_{\boldsymbol{\alpha\beta}}\right) \end{cases} \quad \begin{cases} \frac{\mathrm{d}i_{\mathrm{b}1_\beta}}{\mathrm{d}t} = f_{\alpha\beta_4}\left(\mathbf{u}_{\boldsymbol{\alpha\beta}}, \mathbf{x}_{\boldsymbol{\alpha\beta}}\right) \\ \frac{\mathrm{d}i_{\mathrm{m}\alpha}}{\mathrm{d}t} = f_{\alpha\beta_5}\left(\mathbf{u}_{\boldsymbol{\alpha\beta}}, \mathbf{x}_{\boldsymbol{\alpha\beta}}\right) \\ \frac{\mathrm{d}i_{\mathrm{m}\beta}}{\mathrm{d}t} = f_{\alpha\beta_6}\left(\mathbf{u}_{\boldsymbol{\alpha\beta}}, \mathbf{x}_{\boldsymbol{\alpha\beta}}\right) \end{cases} \tag{14}$$

Here, $\mathbf{u}_{\boldsymbol{\alpha\beta}} = [v_{\mathrm{a}\alpha}, v_{\mathrm{a}\beta}, v_{\mathrm{b}1\alpha}, v_{\mathrm{b}1\beta}]^{\mathrm{T}}$, and $\mathbf{x}_{\boldsymbol{\alpha\beta}} = [i_{\mathrm{a}\alpha}, i_{\mathrm{a}\beta}, i_{\mathrm{b}1\alpha}, i_{\mathrm{b}1\beta}, i_{\mathrm{m}\alpha}, i_{\mathrm{m}\beta}]^{\mathrm{T}}$ represent the input and output vectors in α-β coordinates, respectively. Additionally, $\mathbf{u}_{\boldsymbol{\alpha\beta}} \in \{\mathbb{R}^4\}$ and $\mathbf{x}_{\boldsymbol{\alpha\beta}} \in \{\mathbb{R}^6\}$.

Since the model in (14) is in the α-β rotating frame, Park's transformation can be directly applied. By using the following transformation matrix defined as

$$\mathbf{T} = \begin{bmatrix} \cos\theta & \sin\theta \\ -\sin\theta & \cos\theta \end{bmatrix} \tag{15}$$

where θ is the grid phase angle to (14), the dynamic equations in d-q coordinates are given by (16). From here, $\mathbf{u}_{\mathbf{dq}} = [u_{\mathrm{dq}1}, u_{\mathrm{dq}2}, u_{\mathrm{dq}3}, u_{\mathrm{dq}4}]^{\mathrm{T}} = [v_{\mathrm{ad}}, v_{\mathrm{aq}}, v_{\mathrm{b}1\mathrm{d}}, v_{\mathrm{b}1\mathrm{q}}]^{\mathrm{T}}$, and $\mathbf{x}_{\mathbf{dq}} = [x_{\mathrm{dq}1}, x_{\mathrm{dq}2}, x_{\mathrm{dq}3}, x_{\mathrm{dq}4}, x_{\mathrm{dq}5}, x_{\mathrm{dq}6}]^{\mathrm{T}} = [i_{\mathrm{ad}}, i_{\mathrm{aq}}, i_{\mathrm{b}1\mathrm{d}}, i_{\mathrm{b}1\mathrm{q}}, i_{\mathrm{md}}, i_{\mathrm{mq}}]^{\mathrm{T}}$, with $\mathbf{u}_{\mathbf{dq}} \in \{\mathbb{R}^4\}$ and $\mathbf{x}_{\mathbf{dq}} \in \{\mathbb{R}^6\}$. Evidently, $\mathbf{u}_{\mathbf{dq}}$ and $\mathbf{x}_{\mathbf{dq}}$ represent the input and output vectors in d-q coordinates, respectively.

$$\begin{cases} \frac{\mathrm{d}i_{\mathrm{a}_\mathrm{d}}}{\mathrm{d}t} = f_{\mathrm{dq}_1}\left(\mathbf{u}_{\mathbf{dq}}, \mathbf{x}_{\mathbf{dq}}\right) \\ \frac{\mathrm{d}i_{\mathrm{a}_\mathrm{q}}}{\mathrm{d}t} = f_{\mathrm{dq}_2}\left(\mathbf{u}_{\mathbf{dq}}, \mathbf{x}_{\mathbf{dq}}\right) \\ \frac{\mathrm{d}i_{\mathrm{b}1_\mathrm{d}}}{\mathrm{d}t} = f_{\mathrm{dq}_3}\left(\mathbf{u}_{\mathbf{dq}}, \mathbf{x}_{\mathbf{dq}}\right) \\ \frac{\mathrm{d}i_{\mathrm{b}1_\mathrm{q}}}{\mathrm{d}t} = f_{\mathrm{dq}_4}\left(\mathbf{u}_{\mathbf{dq}}, \mathbf{x}_{\mathbf{dq}}\right) \\ \frac{\mathrm{d}i_{\mathrm{m}_\mathrm{d}}}{\mathrm{d}t} = f_{\mathrm{dq}_5}\left(\mathbf{u}_{\mathbf{dq}}, \mathbf{x}_{\mathbf{dq}}\right) \\ \frac{\mathrm{d}i_{\mathrm{m}\beta}}{\mathrm{d}t} = f_{\mathrm{dq}_6}\left(\mathbf{u}_{\boldsymbol{\alpha\beta}}, \mathbf{x}_{\boldsymbol{\alpha\beta}}\right) \end{cases} \tag{16}$$

By grouping the dynamic equations in (16) into a vector function $\mathbf{f}_{\mathbf{dq}} = [f_{\mathrm{dq}1}(\mathbf{u}_{\mathbf{dq}}, \mathbf{x}_{\mathbf{dq}}), f_{\mathrm{dq}2}(\mathbf{u}_{\mathbf{dq}}, \mathbf{x}_{\mathbf{dq}}), \ldots, f_{\mathrm{dq}6}(\mathbf{u}_{\mathbf{dq}}, \mathbf{x}_{\mathbf{dq}})]^{\mathrm{T}}$ and defining the output vector as $\mathbf{y}_{\mathbf{dq}} = \mathbf{x}_{\mathbf{dq}}$, the state-space model of the 1P-1S system in d-q coordinates is obtained and defined as follows:

$$\begin{cases} \dot{\mathbf{x}}_{\mathrm{dq}} = \mathbf{A}_{\mathbf{dq}} \cdot \mathbf{x}_{\mathbf{dq}} + \mathbf{B}_{\mathbf{dq}} \cdot \mathbf{u}_{\mathbf{dq}} \\ \mathbf{y}_{\mathbf{dq}} = \mathbf{C}_{\mathbf{dq}} \cdot \mathbf{x}_{\mathbf{dq}} + \mathbf{D}_{\mathbf{dq}} \cdot \mathbf{u}_{\mathbf{dq}} \end{cases} \tag{17}$$

It should be noted that $\{\mathbf{f}_{\mathbf{dq}}, \mathbf{y}_{\mathbf{dq}}\} \in \{\mathbb{R}^6\}$. The state matrix $\mathbf{A}_{\mathbf{dq}}$, input matrix $\mathbf{B}_{\mathbf{dq}}$, output matrix $\mathbf{C}_{\mathbf{dq}}$, and direct-transmission matrix $\mathbf{D}_{\mathbf{dq}}$ can be described as follows:

$$\begin{aligned} \mathbf{A}_{\mathbf{dq}} &= \left[\frac{\partial f_{\mathrm{dq}i}(\mathbf{u}_{\mathbf{dq}}, \mathbf{x}_{\mathbf{dq}})}{\partial x_{\mathrm{dq}j}}\right], \quad \mathbf{B}_{\mathbf{dq}} = \left[\frac{\partial f_{\mathrm{dq}i}(\mathbf{u}_{\mathbf{dq}}, \mathbf{x}_{\mathbf{dq}})}{\partial u_{\mathrm{dq}k}}\right], \\ \mathbf{C}_{\mathbf{dq}} &= \left[\frac{\partial x_{\mathrm{dq}i}}{\partial x_{\mathrm{dq}j}}\right], \quad \mathbf{D}_{\mathbf{dq}} = \left[\frac{\partial x_{\mathrm{dq}i}}{\partial u_{\mathrm{dq}k}}\right] \end{aligned} \tag{18}$$

From here, $\{i, j\} \in \{1, 2, 3, 4, 5, 6\}$ and $k \in \{1, 2, 3, 4\}$, and $\mathbf{A}_{\mathbf{dq}} \in \mathscr{M}_{6\times 6}\ \{\mathrm{K}\}$, $\mathbf{B}_{\mathbf{dq}} \in \mathscr{M}_{6\times 4}\ \{\mathrm{K}\}$, $\mathbf{C}_{\mathbf{dq}} \in \mathscr{M}_{6\times 6}\ \{\mathrm{K}\}$, and $\mathbf{D}_{\mathbf{dq}} \in \mathscr{M}_{6\times 4}\ \{\mathrm{K}\}$. The block diagram illustrating the conversion process of the 1P-1S model from ec to d-q is shown in Figure 3a.

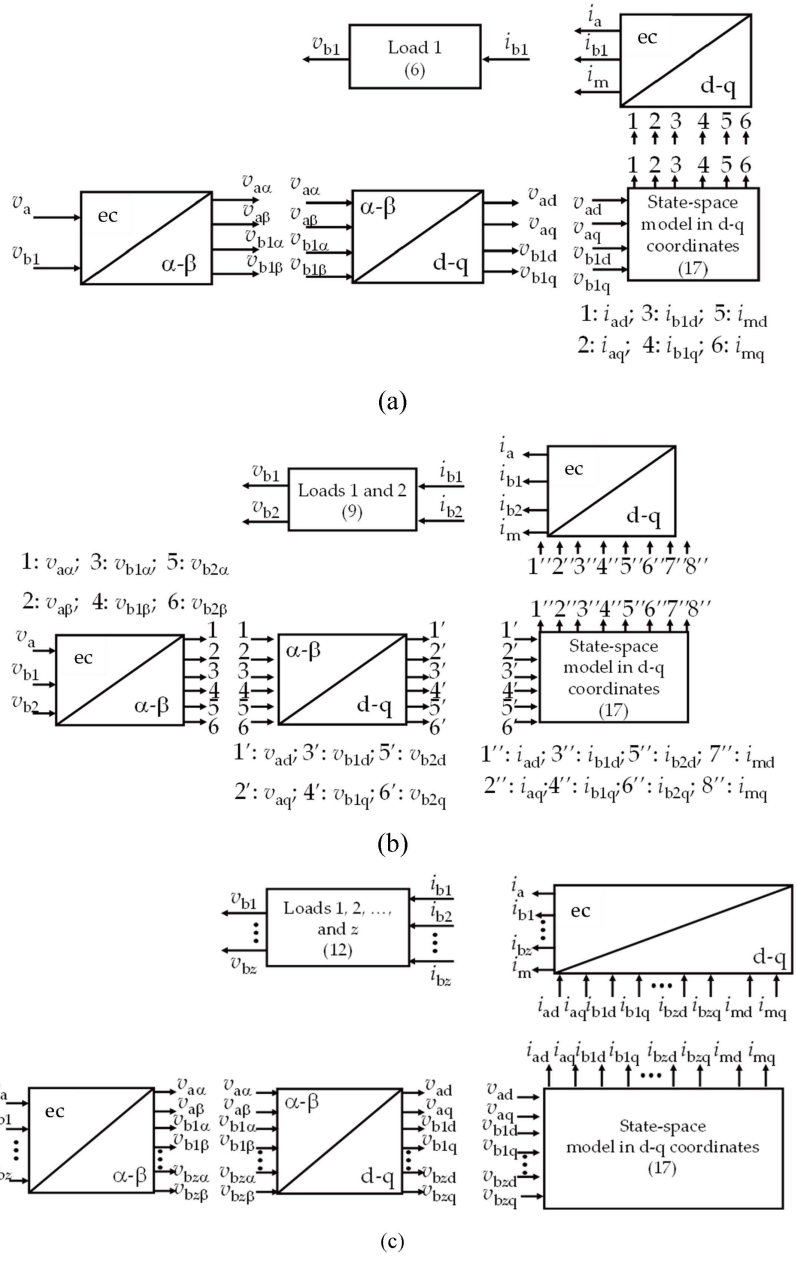

Figure 3. Block diagram of the conversion process for the TRs depicted in Figure 1, in d-q coordinates. (**a**) 1P-1S. (**b**) 1P-2S. (**c**) 1P-*z*S.

4.2 *Dynamic model derivation in d-q coordinates: 1P-2S configuration*

Following a similar procedure, the variables in α-β coordinates for the 1P-2S model are derived as follows

$$\begin{bmatrix} v_{a_\alpha} \\ v_{a_\beta} \\ v_{b_{1\alpha}} \\ v_{b_{1\beta}} \\ v_{b_{2\alpha}} \\ v_{b_{2\beta}} \end{bmatrix} = \begin{bmatrix} v_a(t) \\ v_a(t-\pi/2) \\ v_{b_1}(t) \\ v_{b_1}(t-\pi/2) \\ v_{b_2}(t) \\ v_{b_2}(t-\pi/2) \end{bmatrix}, \quad \begin{bmatrix} i_{a_\alpha} \\ i_{a_\beta} \\ i_{b_{1\alpha}} \\ i_{b_{1\beta}} \\ i_{b_{2\alpha}} \\ i_{b_{2\beta}} \\ i_{m_\alpha} \\ i_{m_\beta} \end{bmatrix} = \begin{bmatrix} i_a(t) \\ i_a(t-\pi/2) \\ i_{b_1}(t) \\ i_{b_1}(t-\pi/2) \\ i_{b_2}(t) \\ i_{b_2}(t-\pi/2) \\ i_m(t) \\ i_m(t-\pi/2) \end{bmatrix} \tag{19}$$

By replacing (19) in (8), the dynamic equations in α-β coordinates for the 1P-2S model are defined by

$$\begin{cases} \frac{di_{a_\alpha}}{dt} = f_{\alpha\beta_1}(\mathbf{u_{\alpha\beta}}, \mathbf{x_{\alpha\beta}}) \\ \frac{di_{a_\beta}}{dt} = f_{\alpha\beta_2}(\mathbf{u_{\alpha\beta}}, \mathbf{x_{\alpha\beta}}) \\ \frac{di_{b_{1\alpha}}}{dt} = f_{\alpha\beta_3}(\mathbf{u_{\alpha\beta}}, \mathbf{x_{\alpha\beta}}) \\ \frac{di_{b_{1\beta}}}{dt} = f_{\alpha\beta_4}(\mathbf{u_{\alpha\beta}}, \mathbf{x_{\alpha\beta}}) \end{cases} \quad \begin{cases} \frac{di_{b_{2\alpha}}}{dt} = f_{\alpha\beta_5}(\mathbf{u_{\alpha\beta}}, \mathbf{x_{\alpha\beta}}) \\ \frac{di_{b_{2\beta}}}{dt} = f_{\alpha\beta_6}(\mathbf{u_{\alpha\beta}}, \mathbf{x_{\alpha\beta}}) \\ \frac{di_{m_\alpha}}{dt} = f_{\alpha\beta_7}(\mathbf{u_{\alpha\beta}}, \mathbf{x_{\alpha\beta}}) \\ \frac{di_{m_\beta}}{dt} = f_{\alpha\beta_8}(\mathbf{u_{\alpha\beta}}, \mathbf{x_{\alpha\beta}}) \end{cases} \tag{20}$$

From here, $\mathbf{u_{\alpha\beta}} = [v_{a\alpha}, v_{a\beta}, v_{b1\alpha}, v_{b1\beta}, v_{b2\alpha}, v_{b2\beta}]^T$, and $\mathbf{x_{\alpha\beta}} = [i_{a\alpha}, i_{a\beta}, i_{b1\alpha}, i_{b1\beta}, i_{b2\alpha}, i_{b2\beta}, i_{m\alpha}, i_{m\beta}]^T$ represent the input and output vectors in α-β coordinates, respectively. Moreover, $\mathbf{u_{\alpha\beta}} \in \{\mathbb{R}^6\}$ and $\mathbf{x_{\alpha\beta}} \in \{\mathbb{R}^8\}$. By applying Park's transformation to (19) using (15), the dynamic model of the 1P-2S system in d-q coordinates is derived and shown as follows

$$\begin{cases} \frac{di_{a_d}}{dt} = f_{dq_1}(\mathbf{u_{dq}}, \mathbf{x_{dq}}) \\ \frac{di_{a_q}}{dt} = f_{dq_2}(\mathbf{u_{dq}}, \mathbf{x_{dq}}) \\ \frac{di_{b_d}}{dt} = f_{dq_3}(\mathbf{u_{dq}}, \mathbf{x_{dq}}) \\ \frac{di_{b_{1q}}}{dt} = f_{dq_4}(\mathbf{u_{dq}}, \mathbf{x_{dq}}) \end{cases} \quad \begin{cases} \frac{di_{b_{2d}}}{dt} = f_{dq_5}(\mathbf{u_{dq}}, \mathbf{x_{dq}}) \\ \frac{di_{b_{2q}}}{dt} = f_{dq_6}(\mathbf{u_{dq}}, \mathbf{x_{dq}}) \\ \frac{di_{m_d}}{dt} = f_{dq_7}(\mathbf{u_{dq}}, \mathbf{x_{dq}}) \\ \frac{di_{m_q}}{dt} = f_{dq_8}(\mathbf{u_{dq}}, \mathbf{x_{dq}}) \end{cases} \tag{21}$$

It should be noted that $\mathbf{u_{dq}} = [u_{dq1}, u_{dq2}, u_{dq3}, u_{dq4}, u_{dq5}, u_{dq6}]^T = [v_{ad}, v_{aq}, v_{b1d}, v_{b1q}, v_{b2d}, v_{b2q}]^T$, and $\mathbf{x_{dq}} = [x_{dq1}, x_{dq2}, x_{dq3}, x_{dq4}, x_{dq5}, x_{dq6}, x_{dq7}, x_{dq8}]^T = [i_{ad}, i_{aq}, i_{b1d}, i_{b1q}, i_{b2d}, i_{b2q}, i_{md}, i_{mq}]^T$ represent the input and output vectors in d-q coordinates, respectively. Moreover, $\mathbf{u_{dq}} \in \{\mathbb{R}^6\}$ and $\mathbf{x_{dq}} \in \{\mathbb{R}^8\}$.

According to (21), defining the output vector in d-q coordinates as $\mathbf{y_{dq}} = \mathbf{x_{dq}}$ and grouping the dynamic equations in (21) into the vector function $\mathbf{f_{dq}} = [f_{dq1}(\mathbf{u_{dq}}, \mathbf{x_{dq}}), f_{dq2}(\mathbf{u_{dq}}, \mathbf{x_{dq}}), ..., f_{dq8}(\mathbf{u_{dq}}, \mathbf{x_{dq}})]^T$, where $\mathbf{f_{dq}} \in \{\mathbb{R}^8\}$, the state-space model of the 1P-2S system in d-q coordinates is obtained and defined in (17). The matrices $\mathbf{A_{dq}}$, $\mathbf{B_{dq}}$, $\mathbf{C_{dq}}$, and $\mathbf{D_{dq}}$ are defined in (18) where $\{i, j\} \in \{1, 2, 3, 4, 5, 6, 7, 8\}$ and $k \in \{1, 2, 3, 4, 5, 6\}$. Also, $\{\mathbf{A_{dq}}, \mathbf{C_{dq}}\} \in \mathscr{M}_{8\times 8}$ {K} and $\{\mathbf{B_{dq}}, \mathbf{D_{dq}}\} \in \mathscr{M}_{8\times 6}$ {K}. The block diagram illustrating the conversion process of the 1P-2S model is depicted in Figure 3b.

4.3 *Dynamic model derivation in d-q coordinates: 1P-zS configuration*

Regarding the generalized 1P-*z*S model, the variables in α-β coordinates are presented and given by

$$\begin{bmatrix} v_{a_\alpha} \\ v_{a_\beta} \\ v_{b_{1\alpha}} \\ v_{b_{1\beta}} \\ v_{b_{2\alpha}} \\ v_{b_{2\beta}} \\ \vdots \\ v_{b_{z\alpha}} \\ v_{b_{z\beta}} \end{bmatrix} = \begin{bmatrix} v_a(t) \\ v_a(t-\pi/2) \\ v_{b_1}(t) \\ v_{b_1}(t-\pi/2) \\ v_{b_2}(t) \\ v_{b_2}(t-\pi/2) \\ \vdots \\ v_{b_z}(t) \\ v_{b_z}(t-\pi/2) \end{bmatrix}, \begin{bmatrix} i_{a_\alpha} \\ i_{a_\beta} \\ i_{b_{1\alpha}} \\ i_{b_{1\beta}} \\ i_{b_{2\alpha}} \\ i_{b_{2\beta}} \\ \vdots \\ i_{b_{z\alpha}} \\ i_{b_{z\beta}} \\ i_{m_\alpha} \\ i_{m_\beta} \end{bmatrix} = \begin{bmatrix} i_a(t) \\ i_a(t-\pi/2) \\ i_{b_1}(t) \\ i_{b_1}(t-\pi/2) \\ i_{b_2}(t) \\ i_{b_2}(t-\pi/2) \\ \vdots \\ i_{b_z}(t) \\ i_{b_z}(t-\pi/2) \\ i_m(t) \\ i_m(t-\pi/2) \end{bmatrix} \tag{22}$$

By replacing (22) in (17), the dynamic equations in α-β coordinates for the generalized 1P-zS model are given by (23). From here, $\mathbf{u_{\alpha\beta}} = [v_{a\alpha}, v_{a\beta}, v_{b1\alpha}, v_{b1\beta}, v_{b2\alpha}, v_{b2\beta}, ..., v_{bz\alpha}, v_{bz\beta}]^T$, and $\mathbf{x_{\alpha\beta}} = [i_{a\alpha}, i_{a\beta}, i_{b1\alpha}, i_{b1\beta}, i_{b2\alpha}, i_{b2\beta}, ..., i_{bz\alpha}, i_{bz\beta}, i_{m\alpha}, i_{m\beta}]^T$ represent the input and output vectors in α-β coordinates, respectively. Moreover, $\mathbf{u_{\alpha\beta}} \in \{\mathbb{R}^{(z+1)}\}$ and $\mathbf{x_{\alpha\beta}} \in \{\mathbb{R}^{(z+3)}\}$.

$$\begin{cases} \frac{di_{a_\alpha}}{dt} = f_{\alpha\beta_1}(\mathbf{u_{\alpha\beta}}, \mathbf{x_{\alpha\beta}}) \\ \frac{di_{a_\beta}}{dt} = f_{\alpha\beta_2}(\mathbf{u_{\alpha\beta}}, \mathbf{x_{\alpha\beta}}) \\ \frac{di_{b_{1\alpha}}}{dt} = f_{\alpha\beta_3}(\mathbf{u_{\alpha\beta}}, \mathbf{x_{\alpha\beta}}) \\ \frac{di_{b_{1\beta}}}{dt} = f_{\alpha\beta_4}(\mathbf{u_{\alpha\beta}}, \mathbf{x_{\alpha\beta}}) \\ \frac{di_{b_{2\alpha}}}{dt} = f_{\alpha\beta_5}(\mathbf{u_{\alpha\beta}}, \mathbf{x_{\alpha\beta}}) \\ \frac{di_{b_{2\beta}}}{dt} = f_{\alpha\beta_6}(\mathbf{u_{\alpha\beta}}, \mathbf{x_{\alpha\beta}}) \\ \vdots \\ \frac{di_{b_{z\alpha}}}{dt} = f_{\alpha\beta_z}(\mathbf{u_{\alpha\beta}}, \mathbf{x_{\alpha\beta}}) \\ \frac{di_{b_{z\beta}}}{dt} = f_{\alpha\beta_{z+1}}(\mathbf{u_{\alpha\beta}}, \mathbf{x_{\alpha\beta}}) \\ \frac{di_{m_\alpha}}{dt} = f_{\alpha\beta_{z+2}}(\mathbf{u_{\alpha\beta}}, \mathbf{x_{\alpha\beta}}) \\ \frac{di_{m_\beta}}{dt} = f_{\alpha\beta_{z+3}}(\mathbf{u_{\alpha\beta}}, \mathbf{x_{\alpha\beta}}) \end{cases} \tag{23}$$

Applying the Park transform to (23), the dynamic equations of the generalized model, defined as functions, in d-q coordinates can be described in (24). Moreover, by grouping the functions in (24), the function vector $\mathbf{f_{dq}} = [f_{dq1}(\mathbf{u_{dq}}, \mathbf{x_{dq}}), f_{dq2}(\mathbf{u_{dq}}, \mathbf{x_{dq}}), \ldots, f_{dq(2+3)}(\mathbf{u_{dq}}, \mathbf{x_{dq}})]^T$ is defined. Also, $\mathbf{f_{dq}} \in \{\mathbb{R}^{z+3}\}$. From (24), $\mathbf{u_{dq}} = [u_{dq1}, u_{dq2}, u_{dq3}, u_{dq4}, u_{dq5}, u_{dq6}, \ldots, u_{dqz}, u_{dq(z+1)}]^T = [v_{ad}, v_{aq}, v_{b1d}, v_{b1q}, v_{b2d}, v_{b2q}, \ldots, v_{bzd}, v_{bzq}]^T$, $\mathbf{x_{dq}} = [x_{dq1}, x_{dq2}, x_{dq3}, x_{dq4}, x_{dq5}, x_{dq6}, x_{dq6}, \ldots, x_{dqz}, x_{dq(z+1)}, x_{dq(z+2)}, x_{dq(z+3)}]^T = [i_{ad}, i_{aq}, i_{b1d}, i_{b1q}, i_{b2d}, i_{b2q}, \ldots, i_{bzd}, i_{bzq}, i_{md}, i_{mq}]^T$ are the input and output vector in d-q coordinates respectively. Moreover, $\mathbf{u_{dq}} \in \{\mathbb{R}^{z+1}\}$ and $\mathbf{x_{dq}} \in \{\mathbb{R}^{z+3}\}$. Also, the matrices $\mathbf{A_{dq}}$, $\mathbf{B_{dq}}$, $\mathbf{C_{dq}}$, and $\mathbf{D_{dq}}$ are defined in (18) taking into account $\{i, j\} \in \{1, 2, \ldots, z, z+1, z+2, z+3\}$ and $k \in \{1, 2, \ldots, z, z+1\}$. Figure 3c shows the conversion process of the generalized 1P- zS model into d-q coordinates.

The sections describe a systematic method for modeling single-phase transformer systems in d-q coordinates, which provides a strong framework for analysis and control. By utilizing Clarke and Park transformations, the dynamic equations are formulated to represent the system seamlessly in the d-q frame. This approach is highly adaptable, accommodating various system configurations and thereby improving the understanding and optimization of power systems. However, increasing the number of secondary windings results in a proportional increase in the number of state variables, particularly those associated with the terminal currents of the secondary windings. To address this challenge, numerous sensors may need to be deployed to accurately measure these variables. Alternatively, an effective solution is to design and implement state observers, which are particularly appropriate in this context given the availability of state-space models [19, 41].

These observers can estimate the system's internal states based on the available measurements, reducing the need for excessive sensors, and providing an efficient solution to handle increased complexity.

$$\begin{cases} \frac{\mathrm{d}i_{\mathrm{a_d}}}{\mathrm{d}t} = f_{\mathrm{dq}_1}\left(\mathbf{u_{dq}},\, \mathbf{x_{dq}}\right) \\ \frac{\mathrm{d}i_{\mathrm{a_q}}}{\mathrm{d}t} = f_{\mathrm{dq}_2}\left(\mathbf{u_{dq}},\, \mathbf{x_{dq}}\right) \\ \frac{\mathrm{d}i_{\mathrm{b}_1\mathrm{d}}}{\mathrm{d}t} = f_{\mathrm{dq}_3}\left(\mathbf{u_{dq}},\, \mathbf{x_{dq}}\right) \\ \frac{\mathrm{d}i_{\mathrm{b}_1\mathrm{q}}}{\mathrm{d}t} = f_{\mathrm{dq}_4}\left(\mathbf{u_{dq}},\, \mathbf{x_{dq}}\right) \\ \frac{\mathrm{d}i_{\mathrm{b}_2\mathrm{d}}}{\mathrm{d}t} = f_{\mathrm{dq}_5}\left(\mathbf{u_{dq}},\, \mathbf{x_{dq}}\right) \\ \frac{\mathrm{d}i_{\mathrm{b}_2\mathrm{q}}}{\mathrm{d}t} = f_{\mathrm{dq}_6}\left(\mathbf{u_{dq}},\, \mathbf{x_{dq}}\right) \\ \vdots \\ \frac{\mathrm{d}i_{\mathrm{b}_z\mathrm{d}}}{\mathrm{d}t} = f_{\mathrm{dq}_z}\left(\mathbf{u_{dq}},\, \mathbf{x_{dq}}\right) \\ \frac{\mathrm{d}i_{\mathrm{b}_z\mathrm{q}}}{\mathrm{d}t} = f_{\mathrm{dq}_{z+1}}\left(\mathbf{u_{dq}},\, \mathbf{x_{dq}}\right) \\ \frac{\mathrm{d}i_{\mathrm{m_d}}}{\mathrm{d}t} = f_{\mathrm{dq}_{z+2}}\left(\mathbf{u_{dq}},\, \mathbf{x_{dq}}\right) \\ \frac{\mathrm{d}i_{\mathrm{m_q}}}{\mathrm{d}t} = f_{\mathrm{dq}_{z+3}}\left(\mathbf{u_{dq}},\, \mathbf{x_{dq}}\right) \end{cases} \tag{24}$$

5. Simulation results

This study simulates three configurations of the models shown in Figure 1: 1P-1S, 1P-2S, and 1P-3S. Table 1 outlines the model parameters for each configuration, allowing the validation of the model proposed in (17) for each case. The simulations are conducted in both PSIM (using ec) and MATLAB-Simulink (employing d-q). Corresponding block diagrams for these implementations, fitted for $z \in \{1, 2, 3\}$, are shown in Figures 4–6.

Table 1. Model Parameters Regarding (1P-1S), (1P-2S), and (1P-3S).

Parameter	Values
R_{a}	12 [mW]
R_{b1}	12.5 [mW]
R_{b2}	14.5 [mW]
R_{b3}	10.5 [mW]
L_{a}	25 [mH[
L_{b1}	35 [mH]
L_{b2}	38 [mH]
L_{b3}	15 [mH]
L_{m}	1 [H]
t_{r1}, t_{r2}, and t_{r3}	1
R_{L1}, R_{L2}, and R_{L3}	10 [W]
L_{L1}, L_{L2}, and L_{L3}	10 [mH]

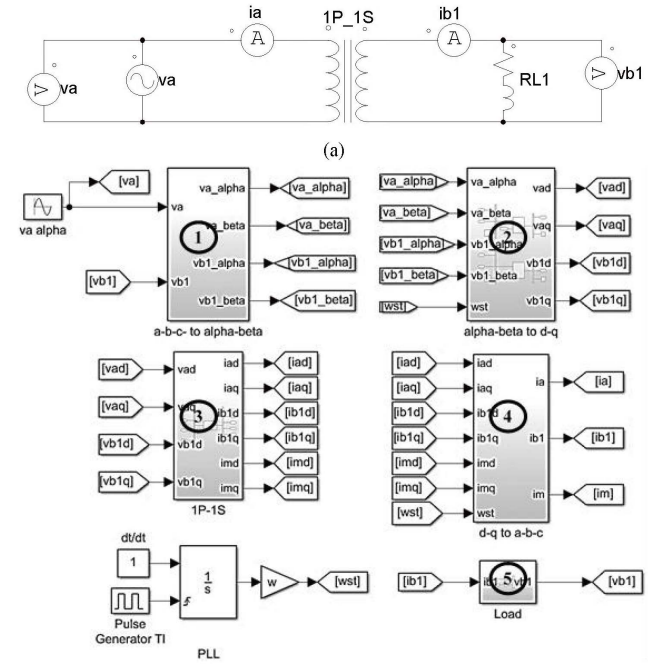

Figure 4. Simulation models regarding 1P-1S implemented using PSIM according to Figure 1 and MATLAB-Simulink according to Figure 3. (**a**) and (**b**) show the implementation of 1P-1S using PSIM and MATLAB-Simulink respectively.

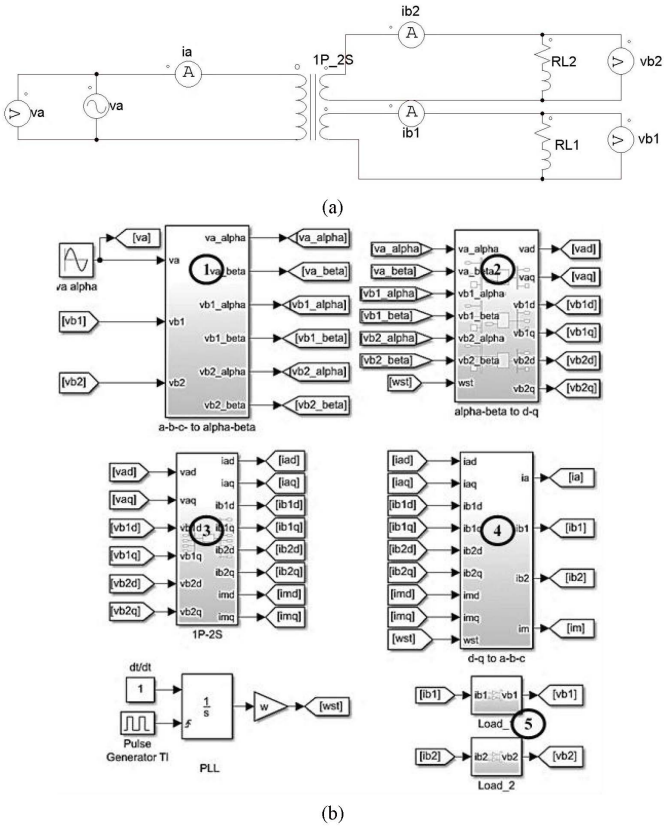

Figure 5. Simulation models regarding 1P-2S implemented using PSIM according to Figure 1 and MATLAB-Simulink according to Figure 3. (**a**) and (**b**) show the implementation of 1P-2S using PSIM and MATLAB-Simulink respectively.

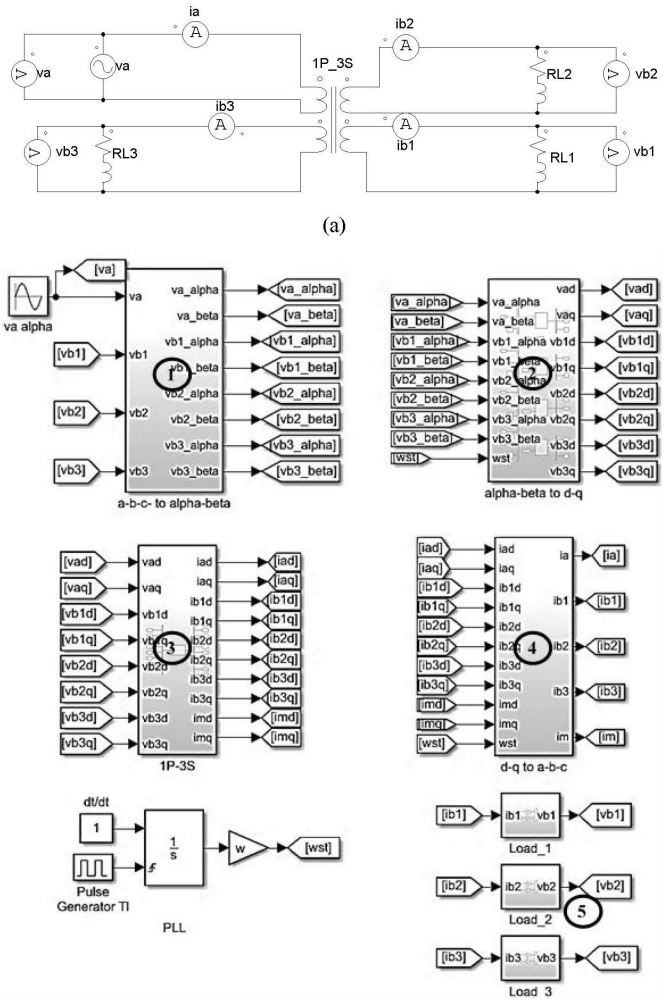

Figure 6. Simulation models regarding 1P-3S implemented using PSIM according to Figure 1 and MATLAB-Simulink according to Figure 3. (**a**) and (**b**) show the implementation of 1P-3S using PSIM and MATLAB-Simulink respectively.

Figures 4a,b–6a,b show the 1P-1S, -2S, and -3S configurations implemented in PSIM and MATLAB-Simulink, respectively. The circuits in PSIM mirror those in Figure 1, while the models in MATLAB-Simulink correspond to the state-space equations depicted in Figure 3. For clarity, a brief explanation of the MATLAB-Simulink models is provided: they consist of blocks representing Clarke linear transformations (converting variables from ec to α-β) and Parks transformations (converting variables from α-β to d-q), along with blocks for configuring the appropriate state-space models (1P-1S, -2S, and -3S) and dynamic equations of the respective loads. In addition, a basic phase-locked loop (PLL) circuit is implemented to control the variable conversion blocks (Clarke and Parks).

Figures 7–9 provides a detailed description of each block shown in Figures 4–6. Specifically, Figures 7a–9a describes the process of converting the variables in ec coordinates to α-β coordinates according to (13), (19), and (22) for $z \in \{1, 2, 3\}$. Meanwhile, Figures 7b–9b implements the system models in d-q-coordinates according to (17) and (18) according to 1P-1S- 2S- and -3S, respectively. Figures 7c–9c demonstrate the conversion of α-β variables to d-q coordinate variables for the 1P-1S, -2S, and -3S models, respectively. Similarly, Figures 7d–9d shows the reconversion of the variables in d-q coordinates to the corresponding ec coordinates in the 1P-1S, -2S, and -3S models, respectively, and finally, Figures 7e–9e details the implementation of the load models of the studied systems according to (6), (9), and (12) for $z \in \{1, 2, 3\}$.

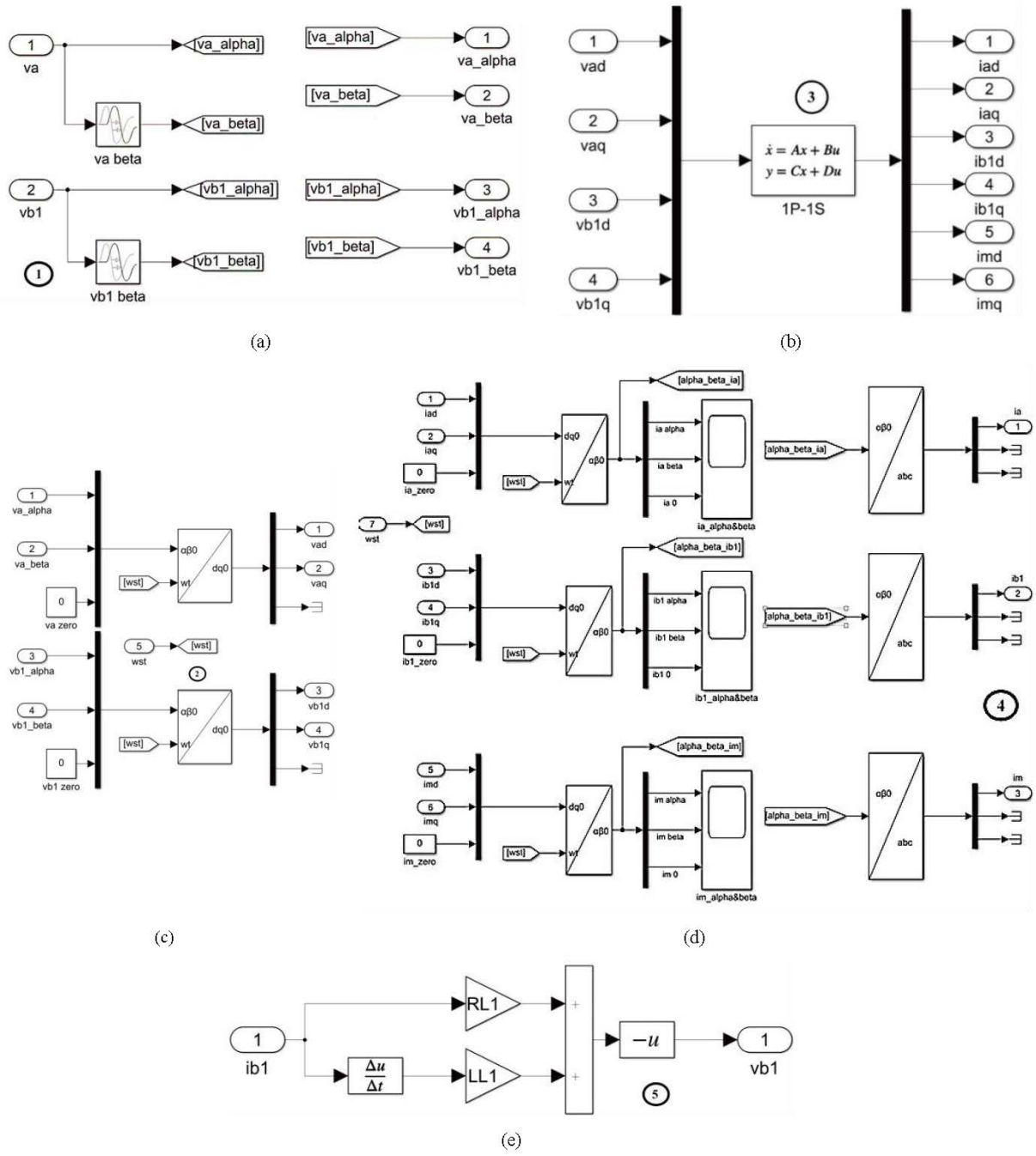

(a) (b) (c) (d) (e)

Figure 7. Details of the blocks shown in Figure 4. (**a**) Block for conversion of variables in ec to -. (**b**) Signal processing of multiple inputs and multiple outputs according to the dynamic model (17). (**c**) Block for converting signals in - coordinates to d-q coordinates. (**d**) Block for reconverting signals in d-q coordinates to ec coordinates. (**e**) Dynamic model of the load described by (6).

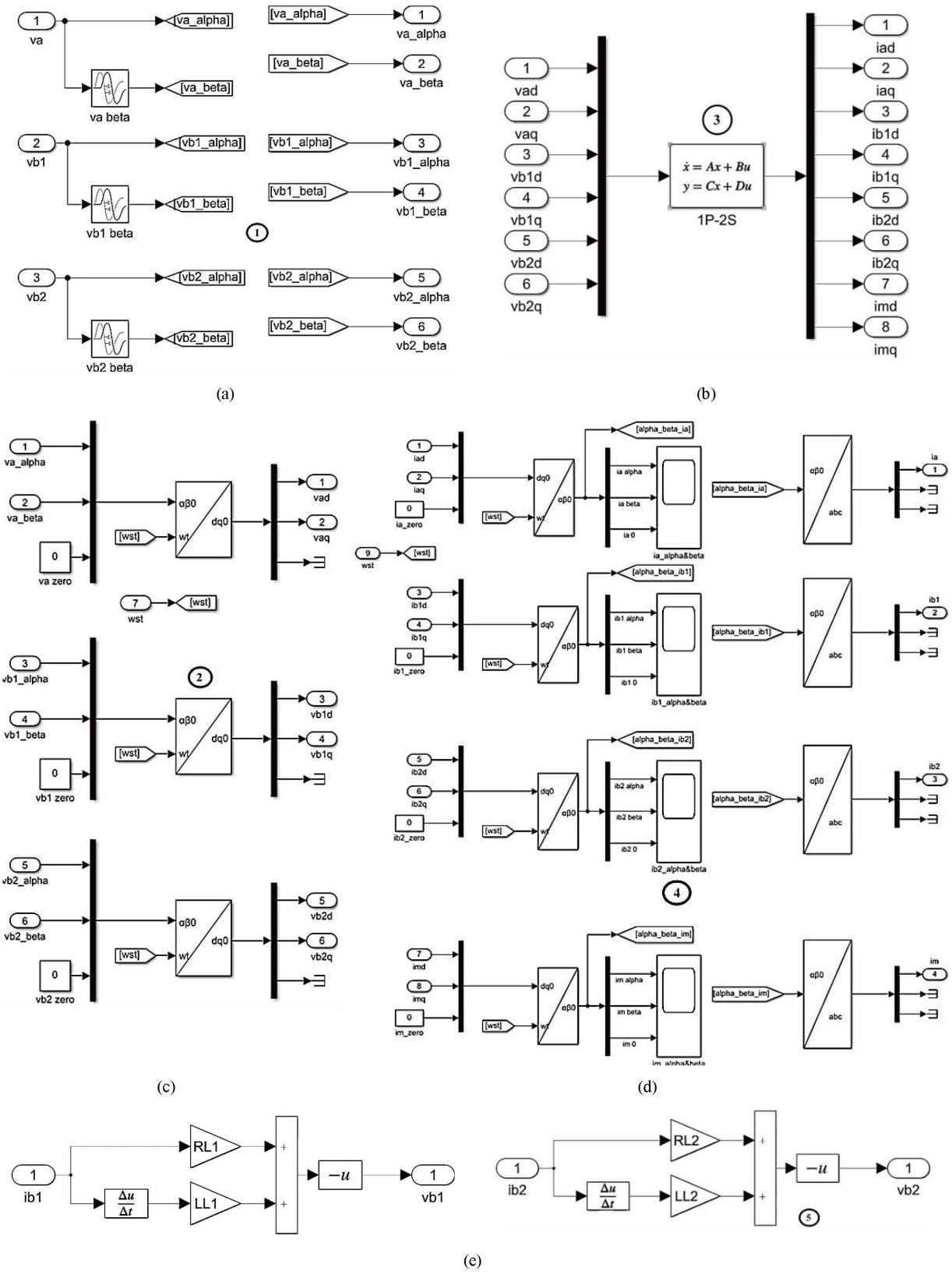

Figure 8. Details of the blocks shown in Figure 4. (**a**) Block for conversion of variables in ec to -. (**b**) Signal processing of multiple inputs and multiple outputs according to the dynamic model (17). (**c**) Block for converting signals in - coordinates to d-q coordinates. (**d**) Block for reconverting signals in d-q coordinates to ec coordinates. (**e**) Dynamic model of the load described by (9).

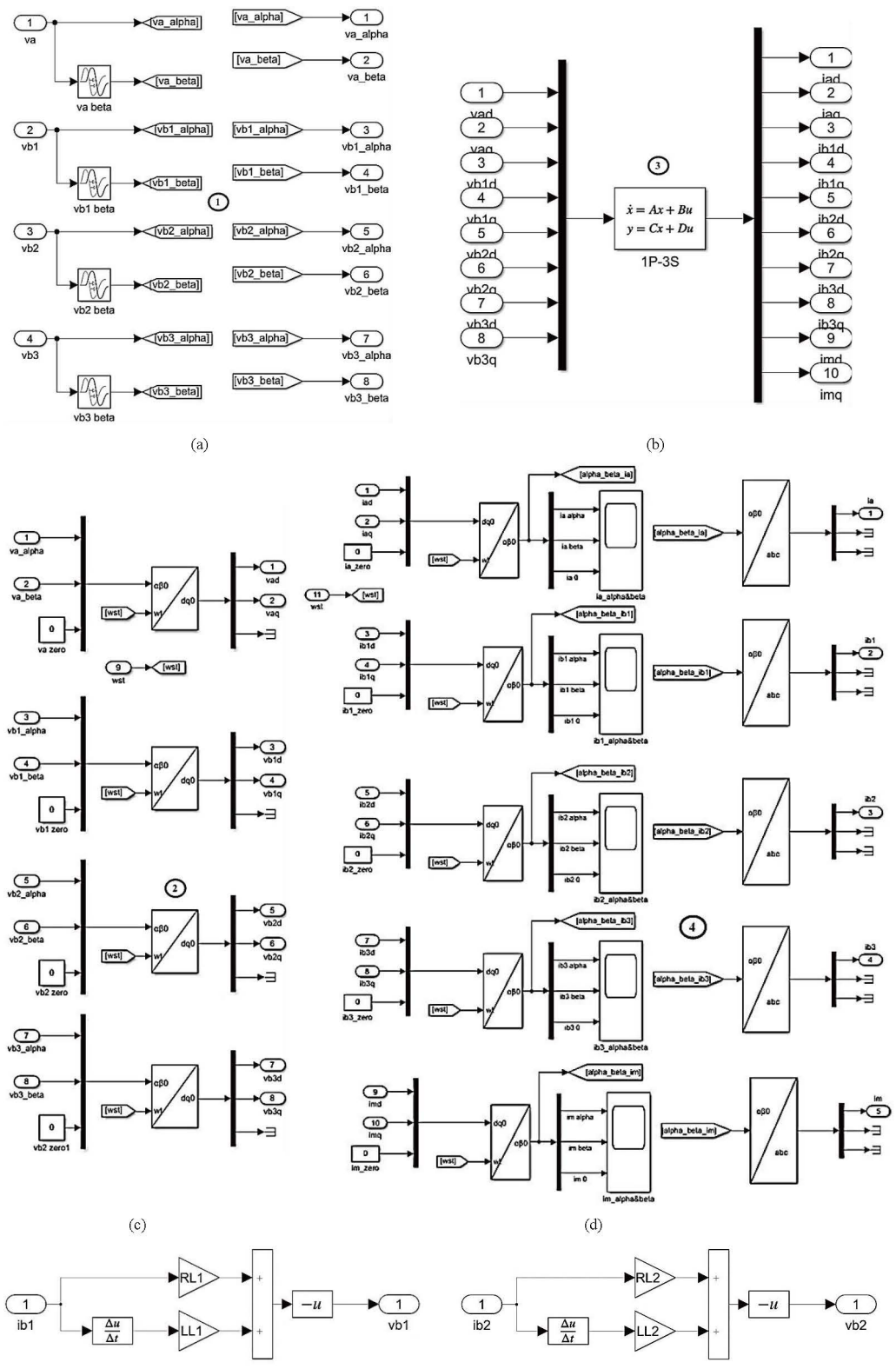

Figure 9. *Cont.*

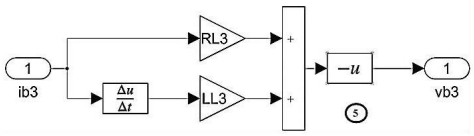

(e)

Figure 9. Details of the blocks shown in Figure 4. (**a**) Block for conversion of variables in ec to α-β. (**b**) Signal processing of multiple inputs and multiple outputs according to the dynamic model (17). (**c**) Block of conversion of signals in α-β coordinates to d-q coordinates. (**d**) Block of reconversion of signals in d-q coordinates to ec coordinates. (**e**) Dynamic model of the load described by (12) with z ∈{1, 2, 3}.

5.1 *Simulation setup*

Each simulation model, whether in PSIM or MATLAB-Simulink, implements a sinusoidal power supply with a peak-to-peak voltage of 311 V at a frequency of 1 kHz, assuming zero initial conditions. It is assumed also, that these inputs are from switching networks coming from any power converter, which pass through a filter tuned to the fundamental frequency of 1 kHz (the frequency at which these models operate), generating an almost pure sinusoidal waveform [18, 42, 43]. It is worth noting that all MATLAB/Simulink simulated models use a fixed-step solver with a fixed step time of t_{step} = 100 ns.

5.2 *Dynamics of 1P-1S system*

Figure 10 shows the transient simulation results for variables v_a, v_{b1}, i_a, and i_{b1} in ec (Figure 10a–d) and d-q variables of v_a, v_{b1}, and i_{b1} (Figure 10e–g) for the 1P-1S system. It is worth noting that the dynamics of these variables in MATLAB-Simulink and PSIM are highly similar, indicating negligible steady-state error. Also, the dynamic behavior of the variables in d-q is similar to that of typical variables in these coordinates, and they appear as constants [44].

Each figure includes a detailed view, which provides an enlarged view of a specific time range. For example, in Figure 10a–d, the zoomed view corresponds to the dynamics of the respective variables when they reach a steady state, i.e., in the range 50 ms $\leq t \leq$60 ms. In the case of the dynamics shown in Figure 10e–f, the zoomed view details the transient response of each of the exposed variables; in this case, $0 \leq t \leq 2$ ms.

5.3 *Dynamics of 1P-2S*

Figure 11 shows the variables v_{bx}, i_a, and i_{bx}, for $x \in \{1, 2\}$in ec coordinates under transient dynamics, i.e., Figure 11a–e respectively, and Figure 12 shows the dynamics in d-q coordinates of v_{bxd}, v_{bxq}, i_{bxd}, and i_{bxq}, under transient dynamics, i.e., Figure 12a–d respectively. It is worth noting that the variables shown in Figure 11 correspond to those obtained from the MATLAB-Simulink model and those obtained from the PSIM model. Furthermore, it is evident that there is a negligible steady-state error. The variables are clearly depicted in Figure 12, with a detailed analysis of their behavior in a steady-state regime in the time range 50 ms $\leq t \leq$ 60 ms, like in the 1P-1S model. Furthermore, details of each of the variables in d-q coordinates can be seen in Figure 12, focusing on the transient stage ($0 \leq t \leq 2$ ms). The dynamic behavior follows the typical form for this type of signal, exhibiting a static characteristic [44].

5.4 *Dynamics of 1P-3S*

Figure 13 describes the dynamics of the variables v_{bx}, i_a, and i_{bx} for $x \in \{1, 2, 3\}$ in coordinates ec under transient regime. The signals shown here are obtained from both the MATLAB-Simulink and PSIM models. Furthermore, Figure 14 illustrates the dynamics of v_{bx} and i_{bx} in d-q coordinates under transient analysis. As in previous cases, Figure 13 demonstrates detailed augmented steady-state dynamics for the time range of 50 ms $\leq t \leq$ 60 ms. Additionally, Figure 14 displays the d-q coordinate dynamics, with enlarged views detailing the transient state of each variable for the time range of $0 \leq t \leq 20$ ms. It is worth noting that the steady-state error remains negligible, consistent with previous models. The dynamic compression of the d-q variables behaves as indicated in the theory [44], presenting a constant gain characteristic.

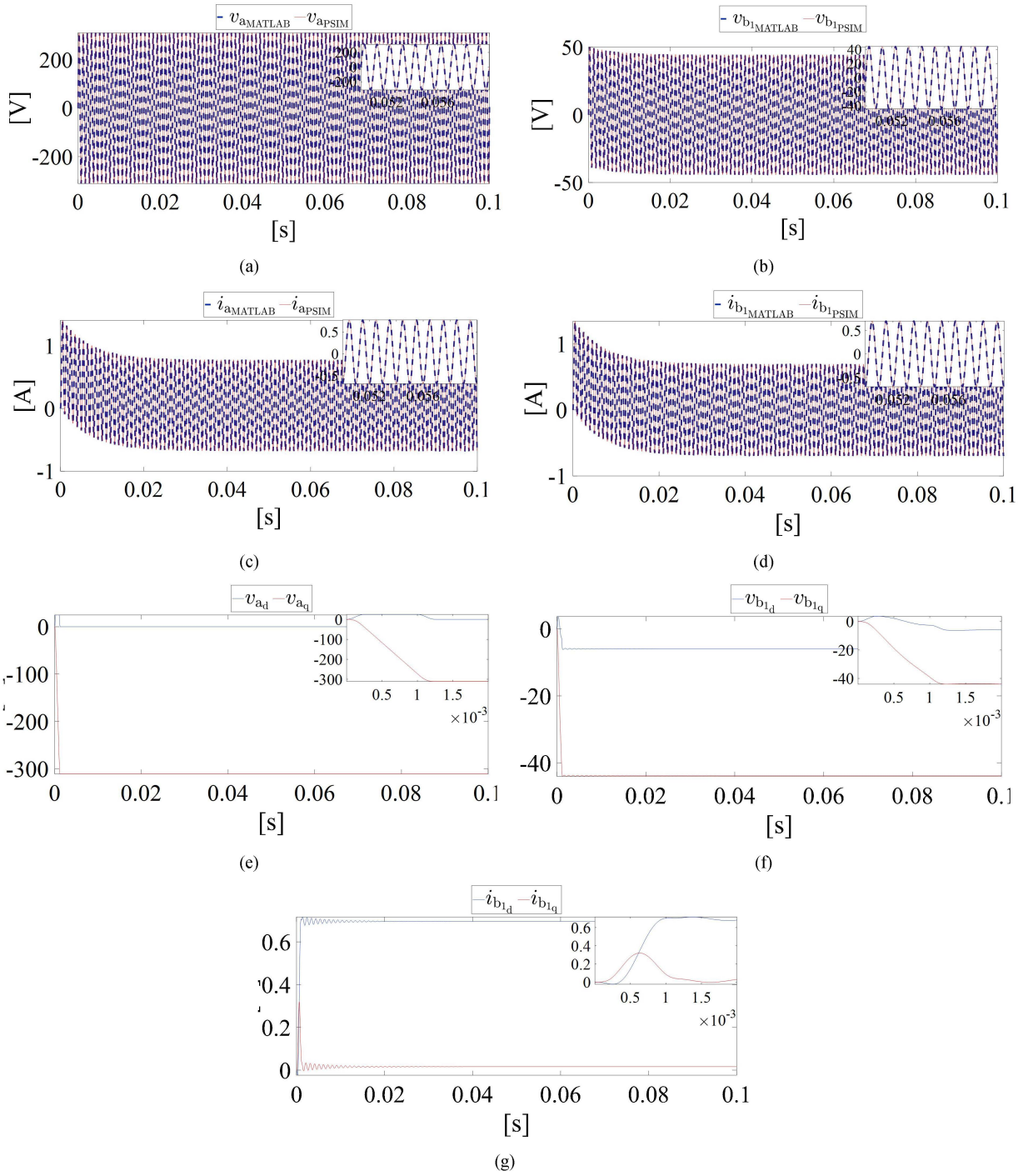

Figure 10. Simulation results under transient's dynamics regarding the operation of the 1P-1S. The initial conditions of all variables are zero. Variables from MATLAB-Simulink are shown in blue and those from PSIM in red according to (**a**)–(**d**). (**a**) Dynamics of v_a. (**b**) Dynamics of v_{b1}. (**c**) Dynamics of i_a. (**d**) Dynamics of i_{b1}. (**e**) Dynamics in d-q coordinates of v_a (v_{ad} and v_{aq}). (**f**) Dynamics in d-q coordinates of v_{b1} (v_{b1d} and v_{b1q}). (**g**) Dynamics in d-q coordinates of i_{b1} (i_{b1d} and i_{b1q}).

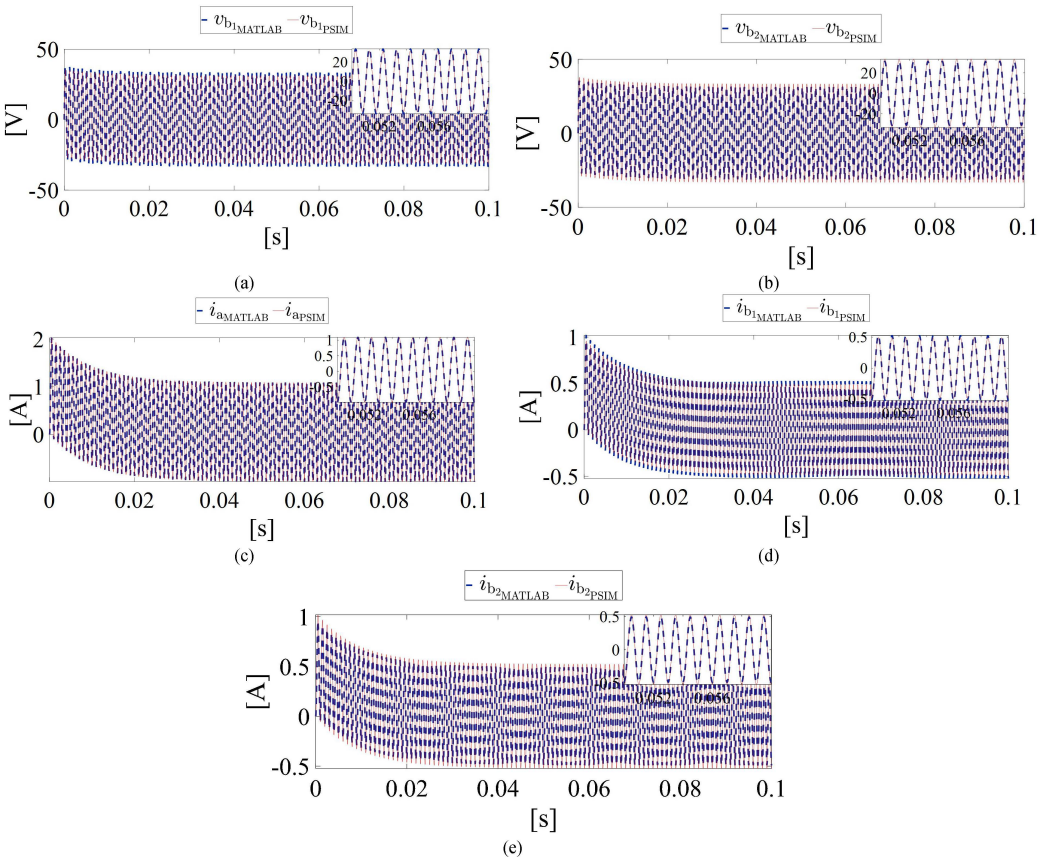

Figure 11. Simulation results under transient's dynamics regarding the operation of the 1P-2S. The initial conditions of all variables are zero. Variables from MATLAB-Simulink are shown in blue and those from PSIM in red. (**a**) Dynamics of v_{b1}. (**b**) Dynamics of v_{b2}. (**c**) Dynamics of i_a. (**d**) Dynamics of i_{b1}. (**e**) Dynamics of i_{b2}.

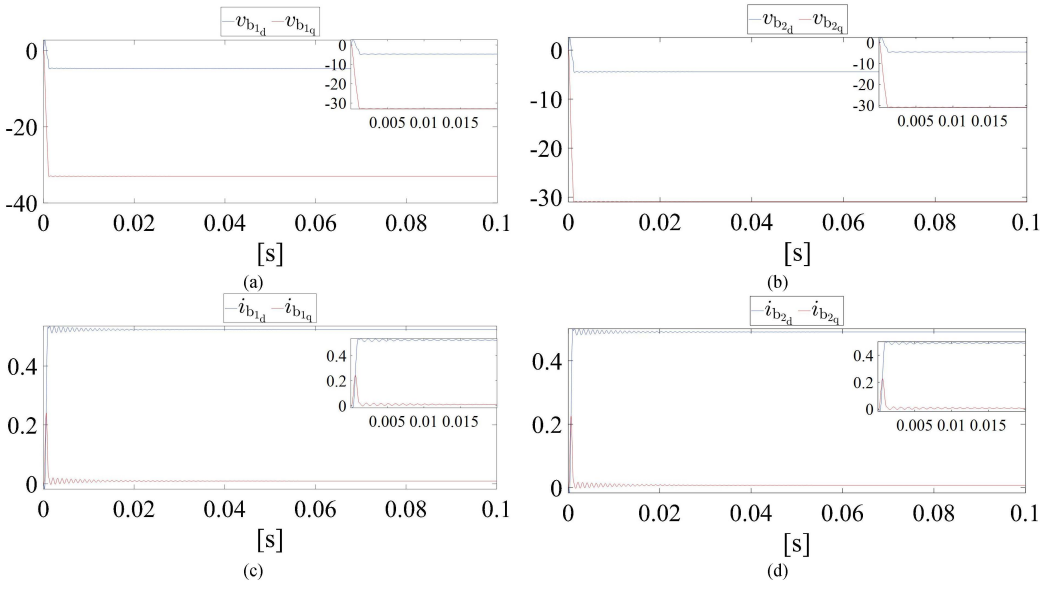

Figure 12. Simulation results under transient's dynamics regarding the operation of the 1P-2S. The initial conditions of all variables are zero. (**a**) Dynamics in d-q coordinates of v_{b1} (v_{b1d} and v_{b1q}). (**b**) Dynamics in d-q coordinates of v_{b2} (v_{b2d} and v_{b2q}). (**c**) Dynamics in d-q coordinates of i_{b1} (i_{b1d} and i_{b1q}). (**d**) Dynamics in d-q coordinates of i_{b2} (i_{b2d} and i_{b2q}).

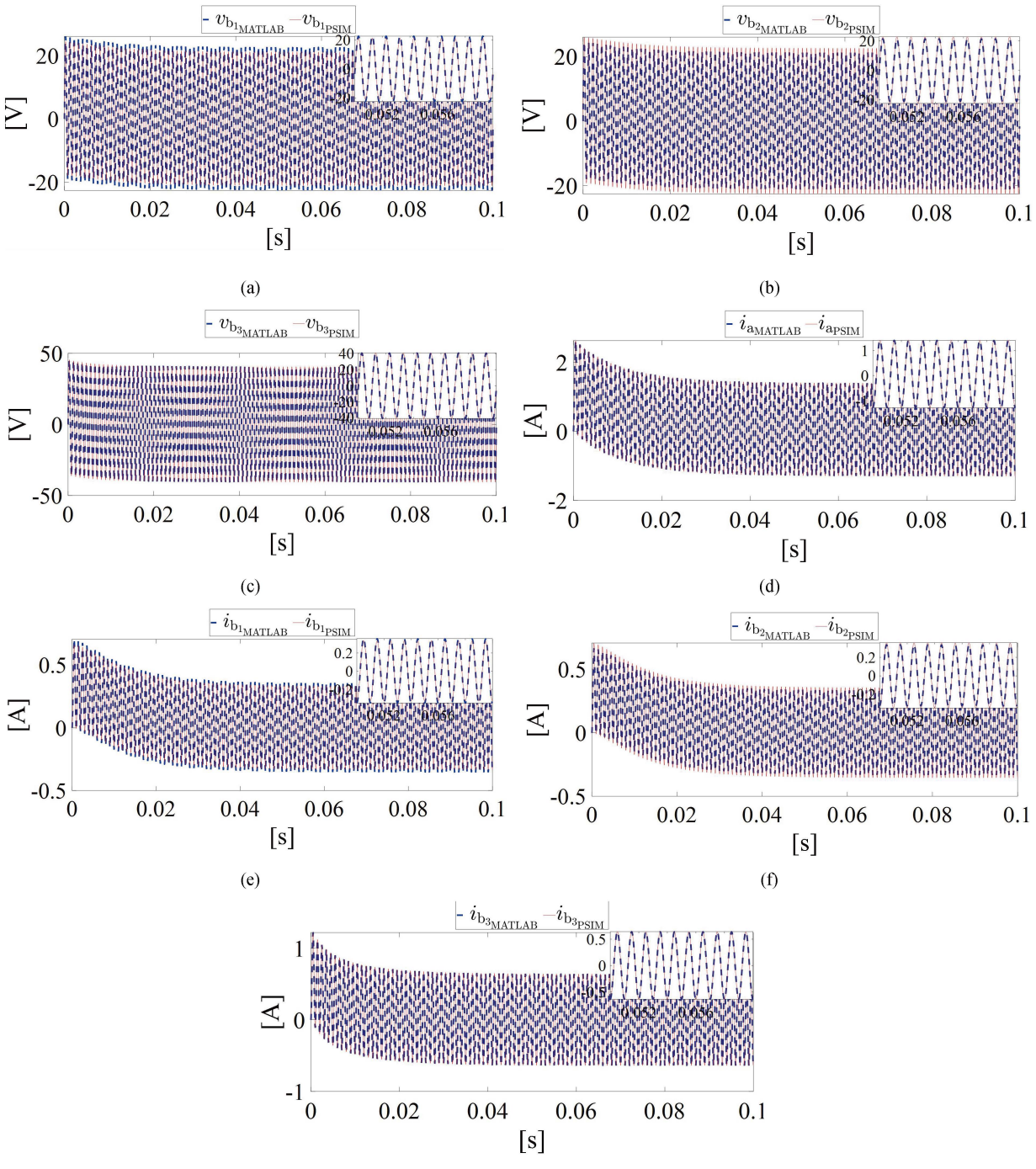

Figure 13. Simulation results under transient dynamics regarding the operation of the 1P-3S. The initial conditions of all variables are zero. Variables from MATLAB-Simulink are shown in blue and those from PSIM in red. (**a**) Dynamics of v_{b1}. (**b**) Dynamics of v_{b2}. (**c**) Dynamics of v_{b3}. (**d**) Dynamics of i_a. (**e**) Dynamics of i_{b1}. (**f**) Dynamics of i_{b2}. (**g**) Dynamics of i_{b3}.

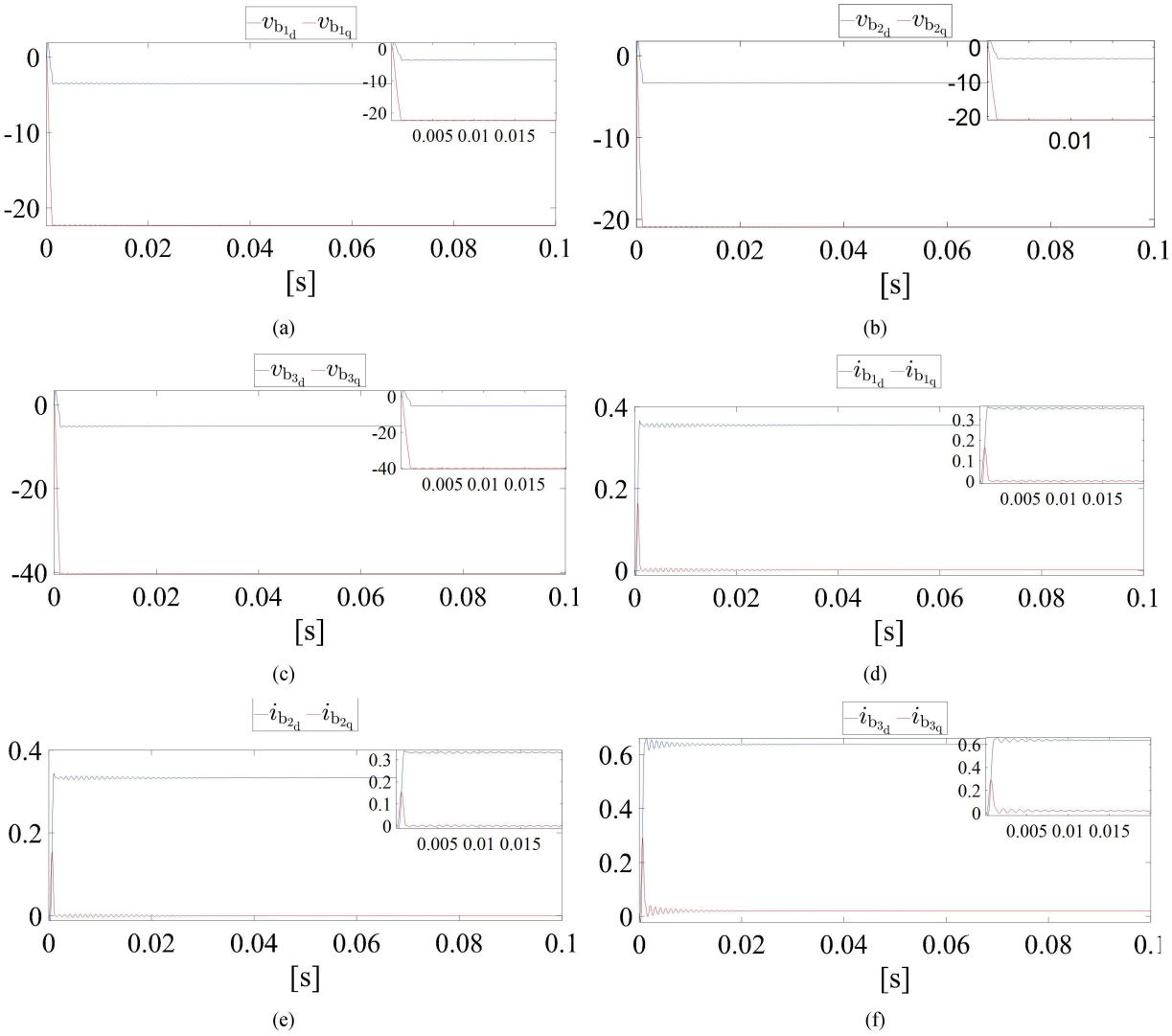

Figure 14. Simulation results under transient's dynamics regarding the operation of the 1P-3S. The initial conditions of all variables are zero. (**a**) Dynamics in d-q coordinates of v_{b1} (v_{b1d} and v_{b1q}). (**b**) Dynamics in d-q coordinates of v_{b2} (v_{b2d} and v_{b2q}). (**c**) Dynamics in d-q coordinates of v_{b3} (v_{b3d} and v_{b3q}). (**d**) Dynamics in d-q coordinates of i_{b1} (i_{b1d} and i_{b1q}). (**e**) Dynamics in d-q coordinates of i_{b2} (i_{b2d} and i_{b2q}). (**f**) Dynamics in d-q coordinates of i_{b3} (i_{b3d} and i_{b3q}).

Table 2 summarizes the steady-state values of electric and dynamic variables in the d-q coordinate system, categorized by system configuration. The low errors obtained through comparisons between electrical variables from MATLAB-Simulink and PSIM confirm the suitability of the state-space models in d-q coordinates for extensive use. This modeling approach provides the basis for synthesizing control systems that can manage power flow across transformer sides, like DABs and SSTs converters. The linear static system's simplicity simplifies control algorithm design, utilizing well-known linear control techniques.

As can be seen in Figure 10e–g, Figures 12 and 14, reaching the steady state is faster for variables in d-q coordinates than for those in ec coordinates. This highlights the significance of using suitable models for d-q dynamics, which can be simulated in shorter times. It is crucial to select the appropriate solver type when generating dynamic simulations in the MATLAB-Simulink environment. It is important to note that changing the solver type from variable step to fixed step together with the type of solver selected: *ode1* (Euler) eliminated the ripple in the variables in dq, as demonstrated in Figures 10–14.

Table 2. Steady-State Values of Electrical and d-q Coordinates of Systems Under Study

System	Variable	Value	Steady-State Error
1P-1S	$v_{a(MATLAB)}$	311 [V peak-to-peak]	0 [V]
	$v_{a(PSIM)}$	311 [V peak-to-peak]	
	$v_{b1(MATLAB)}$	44.28 [V peak-to-peak]	0 [V]
	$v_{b1(PSIM)}$	44.28 [V peak-to-peak]	
	$i_{a(MATLAB)}$	2.0869 [A peak-to-peak]	0 [A]
	$i_{a(PSIM)}$	2.0869 [A peak-to-peak]	
	v_{0ad}	0	-
	v_{aq}	−311	-
	i_{ad}	1.8693 [peak-to-peak]	-
	i_{aq}	1.9244 [peak-to-peak]	-
	v_{b1d}	−5.967	-
	v_{b1q}	−43.88	-
	i_{b1d}	−0.696	-
	i_{b1q}	−0.0159	-
1P-2S	$v_{b1(MATLAB)}$	71.1433 [V peak-to-peak]	4.3727 [V]
	$v_{b1(PSIM)}$	66.7686 [V peak-to-peak]	
	$v_{b2(MATLAB)}$	66.7802 [V peak-to-peak]	4.3489 [V]
	$v_{b2(PSIM)}$	71.1291 [V peak-to-peak]	
	$i_{a(MATLAB)}$	3.0079 [A peak-to-peak]	7.4 [mA]
	$i_{a(PSIM)}$	3.0153 [A peak-to-peak]	
	$i_{b1(MATLAB)}$	1.5425 [A peak-to-peak]	93.3 [mA]
	$i_{b1(PSIM)}$	1.4492 [A peak-to-peak]	
	$i_{b2(MATLAB)}$	1.4493 [A peak-to-peak]	93.3 [mA]
	$i_{b2(PSIM)}$	1.5423 [A peak-to-peak]	
	v_{b1d}	−4.655	-
	v_{b1q}	−32.970	-
	v_{b2d}	−4.421	-
	v_{b2q}	−30.92	-
	i_{b1d}	1.364 [peak-to-peak]	-
	i_{b1q}	1.402 [peak-to-peak]	-
	i_{b2d}	1.2915 [peak-to-peak]	-
	i_{b2q}	1.3232 [peak-to-peak]	-
1P-3S	$v_{b1(MATLAB)}$	48.623 [V peak-to-peak]	3 [V]
	$v_{b1(PSIM)}$	45.6345 [V peak-to-peak]	
	$v_{b2(MATLAB)}$	45.6432 [V peak-to-peak]	3 [V]
	$v_{b2(PSIM)}$	48.6139 [V peak-to-peak]	
	$v_{b3(MATLAB)}$	86.0953 [V peak-to-peak]	14 [mV]
	$v_{b3(PSIM)}$	86.0816 [V peak-to-peak]	
	$i_{a(MATLAB)}$	3.9055 [A peak-to-peak]	8.9 [mA]
	$i_{a(PSIM)}$	3.9144 [A peak-to-peak]	
	$i_{b1(MATLAB)}$	1.0609 [A peak-to-peak]	64.2 [mA]
	$i_{b1(PSIM)}$	0.9967 [A peak-to-peak]	
	$i_{b2(MATLAB)}$	0.9969 [A peak-to-peak]	0.2 [mA]
	$i_{b2(PSIM)}$	1.0608 [A peak-to-peak]	
	$i_{b3(MATLAB)}$	1.8563 [A peak-to-peak]	0.2 [mA]
	$i_{b3(PSIM)}$	1.8561 [A peak-to-peak]	
	v_{b1d}	−3.521	-
	v_{b1q}	−22.32	-
	v_{b2d}	−3.354	-
	v_{b2q}	−20.93	-
	v_{b3d}	−5.152	-
	v_{b3q}	−40.25	-
	i_{b1d}	0.985 [peak-to-peak]	-
	i_{b1q}	0.9923 [peak-to-peak]	-
	i_{b2d}	0.9324 [peak-to-peak]	-
	i_{b2q}	0.9364 [peak-to-peak]	-
	i_{b3d}	1.6159 [peak-to-peak]	-
	i_{b3q}	1.6426 [peak-to-peak]	-

Regarding the matrices defined in (5) and (18), valid for the 1P-1S model, their evaluations according to the values listed in Table 1, are presented below:

$$\mathbf{A_{ec}} = \begin{bmatrix} -0.2040 & 0.2053 & 0 \\ 0.1971 & -0.2105 & 0 \\ -0.0069 & -0.0051 & 0 \end{bmatrix}, \quad \mathbf{B_{ec}} = \begin{bmatrix} 17.0021 & -16.4271 \\ -16.4271 & 16.8378 \\ 0.5749 & 0.4107 \end{bmatrix} \tag{25}$$

$$\mathbf{A_{dq}} = 10^3 \cdot \begin{bmatrix} -0.0002 & 6.2832 & 0.0002 & 0 & 0 & 0 \\ -6.2832 & -0.0002 & 0 & 0.0002 & 0 & 0 \\ 0.0002 & 0 & -0.0002 & 6.2832 & 0 & 0 \\ 0 & 0.0002 & -6.2832 & -0.0002 & 0 & 0 \\ 0 & 0 & 0 & 0 & 0 & 6.2832 \\ 0 & 0 & 0 & 0 & -6.2832 & 0 \end{bmatrix}, \tag{26}$$

$$\mathbf{B_{dq}} = \begin{bmatrix} 17.0021 & 0 & -16.4271 & 0 \\ 0 & 17.0021 & 0 & -16.4271 \\ -16.4271 & 0 & 16.8378 & 0 \\ 0 & -16.4271 & 0 & 16.8378 \\ 0.5749 & 0 & 0.4107 & 0 \\ 0 & 0.5749 & 0 & 0.4107 \end{bmatrix}$$

$$\mathbf{A_{ec}} = \begin{bmatrix} -0.3619 & 0.0879 & 0.0939 & 0.1723 & 0 \\ 0.0844 & -0.2944 & 0.0671 & 0.1230 & 0 \\ 0.0777 & 0.0578 & -0.3198 & 0.1133 & 0 \\ 0.1969 & 0.1465 & -0.3198 & -0.4129 & 0 \\ -0.0030 & -0.0022 & -0.3198 & -0.0043 & 0 \end{bmatrix} \tag{27}$$

$$\mathbf{B_{ec}} = \begin{bmatrix} 30.1571 & -7.0306 & -6.4756 & -16.4048 \\ 7.0306 & 23.5495 & -4.6254 & -11.7177 \\ -6.4756 & -4.6254 & 22.0555 & -10.7926 \\ -16.4048 & -11.7177 & -10.7926 & 39.3253 \\ 0.2461 & 0.1758 & 0.1619 & 0.4101 \end{bmatrix}$$

$$\mathbf{A_{dq}} = 10^3 \cdot \begin{bmatrix} -0.0004 & 6.2832 & 0.0001 & 0 & 0.0001 & 0 & 0.0002 & 0 & 0 & 0 \\ -6.2832 & -0.0004 & 0 & 0.0001 & 0 & 0.0001 & 0 & 0.0002 & 0 & 0 \\ 0.0001 & 0 & -0.0003 & 6.2832 & 0.0001 & 0 & 0.0001 & 0 & 0 & 0 \\ 0 & 0.0001 & -6.2832 & -0.0003 & 0 & 0.0001 & 0 & 0.0001 & 0 & 0 \\ 0.0001 & 0 & 0.0001 & 0 & -0.0003 & 6.2832 & 0.0001 & 0 & 0 & 0 \\ 0 & 0.0001 & 0 & 0.0001 & -6.2832 & -0.0003 & 0 & 0.0001 & 0 & 0 \\ 0.0002 & 0 & 0.0001 & 0 & 0.0002 & 0 & -0.0004 & 6.2832 & 0 & 0 \\ 0 & 0.0002 & 0 & 0.0001 & 0 & 0.0002 & -6.2832 & -0.0004 & 0 & 0 \\ 0 & 0 & 0 & 0 & 0 & 0 & 0 & 0 & 0 & 6.2832 \\ 0 & 0 & 0 & 0 & 0 & 0 & 0 & 0 & -6.2832 & 0 \end{bmatrix}$$

$$\mathbf{B_{dq}} = \begin{bmatrix} 30.1571 & 0 & -7.0306 & 0 & -6.4756 & 0 & -16.4048 & 0 \\ 0 & 30.1571 & 0 & -7.0306 & 0 & -6.4756 & 0 & -16.4048 \\ -7.0306 & 0 & 23.5495 & 0 & -4.6254 & 0 & -11.7177 & 0 \\ 0 & -7.0306 & 0 & 23.5495 & 0 & -4.6254 & 0 & -11.7177 \\ -6.4756 & 0 & -4.6254 & 0 & 22.0555 & 0 & -10.7926 & 0 \\ 0 & -6.4756 & 0 & -4.6254 & 0 & 22.0555 & 0 & -10.7926 \\ -16.4048 & 0 & -11.7177 & 0 & -10.7926 & 0 & 39.3253 & 0 \\ 0 & -16.4048 & 0 & -11.7177 & 0 & -10.7926 & 0 & 39.3253 \\ 0.2461 & 0 & 0.1758 & 0 & 0.1619 & 0 & 0.4101 & 0 \\ 0 & 0.2461 & 0 & 0.1758 & 0 & 0.1619 & 0 & 0.4101 \end{bmatrix} \tag{28}$$

where $\mathbf{C_{ec}} = \mathbf{I_{3\times 3}}$ and $\mathbf{D_{ec}} = \mathbf{0_{3\times 2}}$. Also, the matrices in d-q coordinates can be defined in (26). Similarly, the matrices for the 1P-2S system are described with assurance in (27) and (28). From here, $\mathbf{C_{dq}} = \mathbf{I_{6\times 6}}$ and $\mathbf{D_{ec}} = \mathbf{0_{6\times 4}}$.

Finally, the evaluated matrices corresponding to the 1P-3S system are defined in (27) and (28) respectively, where $\mathbf{C_{dq}} = \mathbf{I_{10\times 10}}$ and $\mathbf{D_{ec}} = \mathbf{0_{10\times 8}}$.

The simulation results confirm the proposed models for 1P-1S, -2S, and -3S configurations, demonstrating close agreement between PSIM and MATLAB-Simulink implementations. Table 1 presents the model parameters, and Figures 4–6 show the corresponding block diagrams. Steady- state simulations in both ec and d-q coordinates exhibit negligible errors, as depicted in Figure 10. Dynamic simulations for 1P-2S and 1P-3S systems demonstrate satisfactory behavior with minimal errors, as shown in Figures 11–14. Although modeling approximations may cause minor ripples in d-q variables, the overall accuracy is maintained. Table 2 summarizes the steady-state values, confirming the suit-ability of d-q coordinate models for control system synthesis, especially for power flow management across transformer sides.

The section on simulation results provides a comprehensive overview of the validation process for the proposed models across various configurations. The study ensures thorough validation and comparison by simulating the 1P-1S, 1P-2S, and 1P-3S setups in both PSIM and MATLAB-Simulink environments. The detailed block diagrams accompanying the explanations facilitate a clear understanding of the simulation setups. The analysis of simulation results, including transient and steady-state dynamics, provides valuable insights into the behavior of the models. The close agreement between PSIM and MATLAB-Simulink simulations underscores the accuracy of the proposed models. Furthermore, the evaluation of steady-state values and matrices provides quantitative validation, reinforcing confidence in the model parameters. The section on solver types provides practical considerations for dynamic simulations, adding depth to the analysis. The presented validation process contributes significantly to the understanding and applicability of the proposed models in power system control.

6. Dynamical equation general solution

This section presents solutions to the dynamic equations of state as presented in (4) and (17). The dynamic model of the governed systems is represented by (4) in ec coordinates, while (17) corresponds to the system in d-q coordinates. These models are linear differential equations that can be confidently solved using the state space representation by obtaining and employing the state transition matrix (Φ) [19, 20, 45].

By modifying the dynamic equations in (4) and (17), they are transformed into non-autonomous forms, described in (29) and (30). From here $\mathbf{A}_{\text{ec}}$ and $\mathbf{A_{dq}}$ are the system matrices corresponding to ec and d-q coordinates respectively, and $\mathbf{B_{ec}}$ and $\mathbf{B_{dq}}$ are the input matrices.

$$\frac{\mathrm{d}\mathbf{x}(t)}{\mathrm{d}t} = \mathbf{A_{ec}} \cdot \mathbf{x}(t) + \mathbf{B_{ec}} \cdot \mathbf{u}(t) \;\Rightarrow\; \frac{\mathrm{d}\mathbf{x}(t)}{\mathrm{d}t} - \mathbf{A_{ec}} \cdot \mathbf{x}(t) = \mathbf{B_{ec}} \cdot \mathbf{u}(t) \tag{29}$$

$$\frac{\mathrm{d}\mathbf{x}_{\text{dq}}(t)}{\mathrm{d}t} = \mathbf{A_{dq}} \cdot \mathbf{x_{dq}}(t) + \mathbf{B_{dq}} \cdot \mathbf{u_{dq}}(t) \Rightarrow \frac{\mathrm{d}\mathbf{x}_{\text{dq}}(t)}{\mathrm{d}t} - \mathbf{A_{dq}} \cdot \mathbf{x}_{\text{dq}}(t) = \mathbf{B_{dq}} \cdot \mathbf{u_{dq}}(t) \tag{30}$$

$$\mathrm{e}^{-\mathbf{A_{ec}} \cdot t} \cdot \frac{\mathrm{d}\mathbf{x}(t)}{\mathrm{d}t} - \mathrm{e}^{-\mathbf{A_{ec}} \cdot t} \cdot \mathbf{A_{ec}} \cdot \mathbf{x}(t) = \mathrm{e}^{-\mathbf{A_{ec}} \cdot t} \cdot \mathbf{B_{ec}} \cdot \mathbf{u}(t) \tag{31}$$

$$\mathrm{e}^{-\mathbf{A_{dq}} \cdot t} \cdot \frac{\mathrm{d}\mathbf{x}_{\text{dq}}(t)}{\mathrm{d}t} - \mathrm{e}^{-\mathbf{A_{dq}} \cdot t} \cdot \mathbf{A_{dq}} \cdot \mathbf{x}_{\text{dq}}(t) = \mathrm{e}^{-\mathbf{A_{dq}} \cdot t} \cdot \mathbf{B_{dq}} \cdot \mathbf{u_{dq}}(t) \tag{32}$$

$$\frac{\mathrm{d}}{\mathrm{d}t}\left(\mathrm{e}^{-\mathbf{A_{ec}} \cdot t} \cdot \mathbf{A_{ec}} \cdot \mathbf{x}(t)\right) = \mathrm{e}^{-\mathbf{A_{ec}} \cdot t} \cdot \mathbf{B_{ec}} \cdot \mathbf{u}(t) \tag{33}$$

$$\frac{\mathrm{d}}{\mathrm{d}t}\left(\mathrm{e}^{-\mathbf{A_{dq}} \cdot t} \cdot \mathbf{A_{dq}} \cdot \mathbf{x}_{\text{dq}}(t)\right) = \mathrm{e}^{-\mathbf{A_{dq}} \cdot t} \cdot \mathbf{B_{dq}} \cdot \mathbf{u_{dq}}(t) \tag{34}$$

Defining $\Phi(t) = \mathrm{e}^{(\mathbf{A}i \cdot t)}$ for $i \in \{\text{ec, dq}\}$ and multiplying both sides of (29) and (30) by $\Phi(-t)$, the following expressions given in (31) and (32) are obtained respectively. The mathematical structures described in (31) and (32) result from applying a derivation using the chain rule, leading to (33) and (34). Integrating both sides of (33) and (34) from 0 to t yields new expressions given by:

$$\begin{aligned} & e^{-\mathbf{A_{ec}}\cdot t}\cdot \mathbf{x}(t)-\mathbf{x}_0=\int_0^t e^{-\mathbf{A_{ec}}\cdot\lambda}\cdot \mathbf{B_{ec}}\cdot \mathbf{u}(t)\cdot d\lambda \\ & \Rightarrow \mathbf{x}(t)=e^{\mathbf{A_{ec}}\cdot t}\cdot \mathbf{x}_0+\int_0^t e^{\mathbf{A_{ec}}\cdot(t-\lambda)}\cdot \mathbf{B_{ec}}\cdot \mathbf{u}(t)\cdot d\lambda \\ & \Rightarrow \mathbf{x}(t)=\mathbf{\Phi}(t)\cdot \mathbf{x}_0+\int_0^t \mathbf{\Phi}(t-\lambda)\cdot \mathbf{B_{ec}}\cdot \mathbf{u}(t)\cdot d\lambda \end{aligned} \tag{35}$$

$$\begin{aligned} & e^{-\mathbf{A_{dq}}\cdot t}\cdot \mathbf{x_{dq}}(t)-\mathbf{x_{dq}}_0=\int_0^t e^{-\mathbf{A_{dq}}\cdot\lambda}\cdot \mathbf{B_{dq}}\cdot \mathbf{u_{dq}}(t)\cdot d\lambda \\ & \Rightarrow \mathbf{x_{dq}}(t)=e^{\mathbf{A_{dq}}\cdot t}\cdot \mathbf{x_{dq}}_0+\int_0^t e^{\mathbf{A_{dq}}\cdot(t-\lambda)}\cdot \mathbf{B_{dq}}\cdot \mathbf{u_{dq}}(t)\cdot d\lambda \\ & \Rightarrow \mathbf{x_{dq}}(t)=\mathbf{\Phi}(t)\cdot \mathbf{x}_0+\int_0^t \mathbf{\Phi}(t-\lambda)\cdot \mathbf{B_{dq}}\cdot \mathbf{u_{dq}}(t)\cdot d\lambda \end{aligned} \tag{36}$$

The initial state conditions of the system, represented by $\mathbf{x_0}$ and $\mathbf{dq_0}$, are considered null for this study, as shown in (35) and (36).

The state transition matrices $\Phi(t)$ are defined by $\Phi(t) = e^{\mathbf{A}i\cdot t} = \mathscr{L}^{-1}\{(s\cdot\mathbf{I}-\mathbf{A}_i)^{-1}\}$, for $i \in \{\text{ec, dq}\}$, where s is the Laplace operator, and $\mathbf{I}$ is the identity matrix of the same size as $\mathbf{A}_i$. With this information, it is possible to solve all the state equations associated with the dynamic models described in (4) and (17). The process begins by obtaining $\Phi(t)$ and then computing it in (35) and (36), thus obtaining the state variables related to Equations (4) and (17).

Due to the large size of the state transition matrices for the 1P-1S, 1P-2S, and 1P-3S models, valid for ec and d-q coordinates, explicit presentation of these matrices is avoided in this subsection.

7. Conclusions

The article provides a comprehensive exploration of system modeling in d-q coordinates for single-phase transformer configurations, meticulously analyzing the complexities of this approach. It begins by highlighting the broad applicability of the d-q transformation in electrical and electronic systems, demonstrating its effectiveness in capturing the dynamics of time-varying systems, even under steady-state conditions. However, the direct application of the d-q transformation to single-phase transformers poses inherent challenges, which the paper addresses.

To overcome these challenges, the study builds on established methodologies by using the Clarke transformation to transform electrical variables from electrical phase coordinates (ec) to α-β coordinates. This transformation, characterized by a 90-degree phase shift and rotation in the α-β plane, provides a more manageable representation of the system. Park's transformation is then used to translate the α-β coordinates into the desired d-q frame, providing a static representation suitable for analysis and control.

A central aspect of the paper is the derivation of dynamic equations in α-β and d-q coordinates, which demonstrates a careful and systematic approach to modeling single-phase transformer systems. By providing these equations in vector-matrix form, the article not only enhances the understanding of system dynamics, but also facilitates efficient analysis and control design. In addition, the inclusion of visually illustrative block diagrams clarify the transformation process, thereby aiding a deeper understanding and visualization of the methodology.

Beyond individual transformer configurations, the analysis includes a generalized 1P-zS model that captures different transformer setups. This enhances the applicability of the modeling approach and highlights its versatility in addressing different system configurations. The adoption of a state-space representation in d-q coordinates, encapsulated by the $\mathbf{A_{dq}}$, $\mathbf{B_{dq}}$, $\mathbf{C_{dq}}$, and $\mathbf{D_{dq}}$ matrices, further enhances the analytical capabilities, enabling researchers and practitioners to gain deeper insights into system behavior and performance. In summary, the article provides a comprehensive and insightful exploration of system modeling in d-q coordinates for single-phase transformer systems, shedding light on a nuanced aspect of power system dynamics and control. Despite its thoroughness, it's important to acknowledge the lack of experimental validation that could further strengthen the applicability of the study to real-world scenarios.

The article provides a comprehensive and informative exploration of system modeling in d-q coordinates for single-phase transformer systems, highlighting a subtle aspect of power system dynamics and control. While it is important to acknowledge the lack of experimental validation, this does not diminish the study's applicability to real-world scenarios.

Conflict of interest

There is no conflict of interest for this study.

References

[1] F. Flores-Bahamonde, H. Renaudineau, A. M. Llor, A. Chub, and S. Kouro, "The DC Transformer Power Electronic Building Block: Powering Next-Generation Converter Design," *IEEE Ind. Electron. Mag.*, vol. 17, pp. 21–35, 2022, https://doi.org/10.1109/MIE.2022.3147168.

[2] C. A. Bulucea, D. A. Nicola, N. E. Mastorakis, and D. C. Cismaru, "Modelling of electrical transformers in dynamic regimes," in *Proc. 9th WSEAS/IASME Int. Conf. Electr. Power Syst., High Voltages, Electr. Mach. (POWER '09)*, Genova, Italy, 2009, pp. 188–195.

[3] M. Shah and K. Ngo, "Parameter extraction for the extended cantilever model of magnetic component windings," *IEEE Trans. Aerosp. Electron. Syst.*, vol. 36, no. 1, pp. 260–266, 2000, https://doi.org/10.1109/7.826328.

[4] J. A. Martinez-Velasco and B. A. Mork, "Transformer modeling for low frequency transients-the state of the art," in *Proc. 2003 IPST Int. Conf. Power Syst. Transients*, New Orleans, USA, 2003, pp. 1–6.

[5] J. G. Hayes, N. O'Donovan, and M. G. Egan, "The extended T model of the multiwinding transformer," in *Proc. 2004 IEEE 35th Annu. Power Electron. Spec. Conf. (IEEE Cat. No. 04CH37551)*, Aachen, Germany, 2004, pp. 1812–1817, https://doi.org/10.1109/PESC.2004.1355391.

[6] R. W. Erickson and D. Maksimovic, "A multiple-winding magnetics model having directly measurable parameters," in *Proc. PESC 98 Rec. 29th Annu. IEEE Power Electron. Spec. Conf. (Cat. No. 98CH36196)*, Fukuoka, Japan, 1998, pp. 1472–1478, https://doi.org/10.1109/PESC.1998.703254.

[7] L. Li, G. Xu, D. Sha, Y. Liu, Y. Sun, and M. Su, "Review of Dual-Active-Bridge Converters With Topological Modifications," *IEEE Trans. Power Electron.*, vol. 38, pp. 9046–9076, 2023, https://doi.org/10.1109/TPEL.2023.3258418.

[8] M. Kang, P. Enjeti, and I. Pitel, "Analysis and design of electronic transformers for electric power distribution system," *IEEE Trans. Power Electron.*, vol. 14, no. 6, pp. 1133–1141, 1999, https://doi.org/10.1109/63.803407.

[9] M. Monika, R. Meshram, S. Wagh, N. M. Singh, and A. M. Stanković, "Robust Control of Solid State Transformer using Dynamic Phasor based model with dq transformation," in *Proc. 2019 North Am. Power Symp. (NAPS)*, Wichita, KS, USA, 2019, pp. 1–6, https://doi.org/10.1109/NAPS46351.2019.9000398.

[10] C. Mao, D. Wang, and J. Lu, "The Research on Special Electronic Power Transformer," *IU J. Electr. Electron. Eng.*, vol. 9, pp. 895–903, 2009.

[11] E. I. Amoiralis, M. A. Tsili, and A. G. Kladas, "Transformer Design and Optimization: A Literature Survey," *IEEE Trans. Power Deliv.*, vol. 24, no. 4, pp. 1999–2024, 2009, https://doi.org/10.1109/TPWRD.2009.2028763.

[12] H. Shadfar, M. G. Pashakolaei, and A. A. Foroud, "Solid-state transformers: An overview of the concept, topology, and its applications in the smart grid," *Int. Trans. Electr. Energy Syst.*, vol. 31, no. 11, p. e12996, 2021, https://doi.org/10.1002/2050-7038.12996.

[13] S. Busquets Monge, "Neutral-point-clamped dc-ac power converters," in *Wiley Encyclopedia of Electrical and Electronics Engineering*. Hoboken, NJ, USA: Wiley-Interscience. 2018, pp. 1–20, https://doi.org/10.1002/047134608X.W8365.

[14] A. E. Fitzgerald, C. Kingsley, and S. D. Umans, *Electric Machinery*. New York, NY, USA: McGraw-Hill, 2003.

[15] W. Stevenson Jr and J. Grainger, *Power System Analysis*. New York, NY, USA: McGraw-Hill, 1994.

[16] F. Blaabjerg, "Power Electronics Converters—An Overview," in *Control of Power Electronic Converters and Systems Volume 2*. London, UK: Academic Press, 2018.

[17] N. Mohan, T. M. Undeland, and W. P. Robbins, *Power Electronics: Converters, Applications, and Design*. Hoboken, NJ, USA: John Wiley & Sons, 2003.

[18] R. W. Erickson and D. Maksimovic, *Fundamentals of Power Electronics*. Berlin/Heidelberg, Germany: Springer Science & Business Media, 2007.

[19] K. Ogata, *Modern Control Engineering*. Havana, Cuba: Editorial Félix Varela, 2009.
[20] B. C. Kuo, *Automatic Control Systems*, 6th ed. Englewood Cliffs, NJ, USA: Prentice Hall, 1987.
[21] Z. Zou, M. Liserre, Z. Wang, and M. Cheng, "Modeling and stability analysis of a smart transformer-fed grid," *IEEE Access*, vol. 8, pp. 91876–91885, 2020, https://doi.org/10.1109/ACCESS.2020.2993558.
[22] F. Tidner, "Development and Analysis of Small Signal DQ-Frame Model for Low Frequency Stability of Train Converters," M.S. Dissertation, KTH Royal Inst. Technol., Stockholm, Sweden, 2023.
[23] L. Fan, Z. Miao, P. Koralewicz, S. Shah, and V. Gevorgian, "Identifying DQ-Domain Admittance Models of a 2.3-MVA Commercial Grid-Following Inverter via Frequency-Domain and Time-Domain Data," *IEEE Trans. Energy Convers.*, vol. 36, no. 3, pp. 2463–2472, 2020, https://doi.org/10.1109/TEC.2020.3048389.
[24] Y. Levron, J. Belikov, and D. Baimel, "A Tutorial on Dynamics and Control of Power Systems with Distributed and Renewable Energy Sources Based on the DQ0 Transformation," *Appl. Sci.*, vol. 8, no. 9, p. 1661, 2018, https://doi.org/10.3390/app8091661.
[25] O. M. Hebala, A. A. Aboushady, K. H. Ahmed, S. Burgess, and R. Prabhu, "Generalized small-signal modelling of dual active bridge DC/DC converter," in *Proc. 2018 7th Int. Conf. Renew. Energy Res. Appl. (ICRERA)*, Paris, France, 2018, pp. 914–919, https://doi.org/10.1109/ICRERA.2018.8567014.
[26] B. C. Trento, "Modeling and Control of Single Phase Grid-Tie Converters," M.S. Thesis, Univ. TN, Knoxville, TN, USA, 2012.
[27] N. Mohan, *Electric Machines and Drives*. Hoboken, NJ, USA: Wiley, 2012.
[28] J. A. Edminister and M. Nahvi, *Schaum's Outline of Electromagnetics*. New York, NY, USA: McGraw Hill, 2014.
[29] S. Chapman, *Electric Machinery Fundamentals*, 5th ed. New York, NY, USA: McGraw Hill, 2004.
[30] J. Fraile Mora, *Máquinas eléctricas*. Cuenca, Ecuador: Universidad del Azuay, 2015.
[31] B.-H. Kwon, J.-H. Youm, and J.-W. Lim, "A line-voltage-sensorless synchronous rectifier," *IEEE Trans. Power Electron.*, vol. 14, no. 5, pp. 966–972, 1999, https://doi.org/10.1109/63.788502.
[32] S. Alepuz, S. Busquets-Monge, J. Bordonau, J. Gago, D. Gonzalez, and J. Balcells, "Interfacing Renewable Energy Sources to the Utility Grid Using a Three-Level Inverter," *IEEE Trans. Ind. Electron.*, vol. 53, no. 5, pp. 1504–1511, 2006, https://doi.org/10.1109/TIE.2006.882021.
[33] S. Alepuz, J. Bordonau, and J. Peracaula, "Dynamic analysis of three-level voltage-source inverters applied to power regulation," in *Proc. 30th Annu. IEEE Power Electron. Specialists Conf. (PESC)*, Charleston, SC, USA, 1999, pp. 721–726, https://doi.org/10.1109/PESC.1999.785589.
[34] T. Habetler, "A space vector-based rectifier regulator for AC/DC/AC converters," *IEEE Trans. Power Electron.*, vol. 8, no. 1, pp. 30–36, 1993, https://doi.org/10.1109/63.208497.
[35] T. Habetler and D. Divan, "Angle controlled current regulated rectifiers for AC/AC converters," *IEEE Trans. Power Electron.*, vol. 6, no. 3, pp. 463–469, 1991, https://doi.org/10.1109/63.85914.
[36] S. Hiti, D. Boroyevich, and C. Cuadros, "Small-signal modeling and control of three-phase PWM converters," in *Proc. 1994 IEEE Ind. Appl. Soc. Annu. Meet.*, Denver, CO, USA, 1994, pp. 1143–1150, https://doi.org/10.1109/IAS.1994.377572.
[37] N. Celanovic and D. Boroyevich, "A comprehensive study of neutral-point voltage balancing problem in three-level neutral-point-clamped voltage source PWM inverters," *IEEE Trans. Power Electron.*, vol. 15, no. 2, pp. 242–249, 2000, https://doi.org/10.1109/63.838096.
[38] M. Waqas, T. Ahmed, R. M. Elavarasan, A. Waqar, K. Leong, R. Pugazhendhi, and M. W. Jeelani, "DQ transformation based control of single-phase grid-tied inverter," in *Proc. 2021 31st Australasian Univ. Power Eng. Conf. (AUPEC)*, Perth, Australia, 2021, pp. 1–6, https://doi.org/10.1109/AUPEC52110.2021.9597712.
[39] D. Katole, M. Daigavane, S. Gawande, and P. Daigavane, "Analysis, Design and Implementation of Single Phase SRF Controller for Dynamic Voltage Restorer under Distorted Supply Condition," *Energy Procedia*, vol. 117, pp. 716–723, 2017, https://doi.org/10.1016/j.egypro.2017.05.186.
[40] B. Crowhurst, E. F. El-Saadany, L. El Chaar, and L. A. Lamont, "Single-phase grid-tie inverter control using DQ transform for active and reactive load power compensation," in *Proc. 2010 IEEE Int. Conf. Power Energy*, Kuala Lumpur, Malaysia, 2010, pp. 489–494, https://doi.org/10.1109/PECON.2010.5697632.

[41] P. Dorato, V. Cerone, and C. Abdallah, *Linear Quadratic Control: An Introduction*. Malabar, FL, USA: Krieger Publishing Company, 2000.

[42] F. Kuo, *Network Analysis and Synthesis*. Hoboken, NJ, USA: John Wiley & Sons, 2006.

[43] S. Franco, *Design with Operational Amplifiers and Analog Integrated Circuits*, 3rd ed. New York, NY, USA: McGraw-Hill, 2002.

[44] C. J. O'Rourke, M. M. Qasim, M. R. Overlin, and J. L. Kirtley, "A Geometric Interpretation of Reference Frames and Transformations: dq0, Clarke, and Park," *IEEE Trans. Energy Convers.*, vol. 34, no. 4, pp. 2070–2083, 2019, https://doi.org/10.1109/TEC.2019.2941175.

[45] W. L. Brogan, *Modern Control Theory*, 3rd ed. Chennai, India: Pearson Education India, 1991.